



Norwegian University
of Life Sciences

Master's Thesis 30 ECTS

Faculty of Science and Technology
Geir Halnes

Exploring the Electric Diffusion Potential in the Extracellular Space of the Brain

Sigrid Videm

Natural Science with Teacher Education
Faculty of Science and Technology

Acknowledgements

I would like to thank my supervisor Geir Halnes for his keen interest in my project, his extreme patience, and for valuable feedback. My co-supervisor Andreas Solbrå has a computational expertise and passion for accuracy that have been both helpful and inspiring. I am in debt to Torbjørn V. Ness for useful input, and Sergey Gratiy for sharing data and code from his projects.

My husband, Erlend Aune, has provided moral and technical support throughout this semester.

I also want my parents, and my friends Rolf and Benedicte, to know that they have contributed a lot to my well-being while writing this thesis.

Abstract

Intense neuronal signalling may locally change the ionic composition of the extracellular space, and produce ionic concentration gradients. The ionic concentration gradients causes an electric diffusion potential, described by the Nernst–Planck equation. I have modelled this diffusion potential, by combining the Nernst–Planck equation with Kirchoff’s law of current conservation, this is what is called the Kirchoff–Nernst–Planck-formalism [1][2]. By assuming a laminar structure of the cortex, I made a one-dimensional model of the diffusion potential. The potential was simulated by implementing a numerical scheme in Python. I have found recorded concentration profiles from previously published experiments, where the extracellular concentration gradients were high, but not pathologically high. I used these concentration profiles as initial conditions. The aim of this project has been to investigate whether the diffusion potential makes up a measurable part of the extracellular potential. From previous studies [2][3], I know that the diffusion potential has low frequencies, and its effect would be in the low-frequency part of the extracellular potential – the local field potential. The frequencies of the local field potential were analyzed by computing the power spectrum density. I found that for recordable frequencies (from 0.3 Hz and above) and non-pathological ion concentration gradients, the diffusion potential was much smaller than measured local field potential.

The concentration gradients are transient, and the baseline concentrations are re-established approximately hundred times faster than what diffusion accounts for [4]. I simulated a diffusion potential caused by exponentially decaying concentration gradients, with typical half-lives from previous experiments. This produced a diffusion potential with higher powers in the range of the recordable frequencies, but still not at the level of the recorded local field potential.

Some pathological conditions are associated with extreme concentration

gradients. I have used a recorded concentration profile where the deviations from baseline concentrations were approximately ten times higher than the non-pathological concentration deviations. I saw that in this case, the diffusion potential was of the same magnitude as the local field potential, and even larger, for frequencies lower than approximately 2 Hz. I also tried this extreme scenario with exponentially decaying concentration gradients. This resulted in a diffusion potential which was larger than the local field potential for almost all frequencies in the range of the simulation.

Contents

1	Introduction	1
2	Background	6
2.1	Ionic concentrations and neuronal signalling	6
2.1.1	The resting membrane potential	6
2.1.2	Action potentials	7
2.1.3	Deviation from electroneutrality	8
2.1.4	Intercellular signalling	8
2.2	Layered structures in the brain	8
2.3	Local Field Potentials	10
2.4	The Nernst–Planck equation	11
2.5	The diffusion potential	12
2.6	Electrodiffusion in the extracellular space	14
2.7	Previously published extracellular concentration recordings .	15
2.7.1	Laminar concentration profiles	15
2.7.2	Concentrations of the other ion species	16
2.7.3	The time course of the $[K^+]$ decay	16
2.8	The power spectrum density	18
2.9	Spreading depression	19
2.10	An analytical solution of a simplified system	20
2.10.1	The effective diffusion coefficient of a two-ion system .	20
2.10.2	The analytical solution to the one dimensional diffusion equation	21

3 Methods	23
3.1 Numerical scheme for solving the 1D Nernst–Planck equation	23
3.2 Implementation of the numerical scheme	25
3.3 Initial concentration profiles based on recorded ionic concentrations	26
3.4 The solution and its power spectrum density	28
3.5 The quality of the solver	29
4 Results	31
4.1 Error analysis	31
4.2 Evaluation of the scenarios for the initial concentration profiles	34
4.2.1 The shape of the diffusion potential at $t = 0$	35
4.2.2 The PSD of the diffusion potential	36
4.3 The diffusion potentials calculated from K^+ profiles from four different experiments	37
4.3.1 The shape of the initial concentration profile and of the diffusion potential	37
4.3.2 The PSD of the diffusion potential	39
4.3.3 The PSD of the diffusion potential compared to PSDs of local field potentials	41
4.4 Exponential $\Delta[K^+]$ decay	43
4.5 Spreading depression	46
5 Discussion	48
5.1 Properties of the diffusion potential	48
5.2 The effect of the diffusion potential on the local field potential	49
6 Bibliography	51

Chapter 1

Introduction

The field of neuroscience is as branched as the neuron itself. It encloses anatomy, physiology, biochemistry, cell biology, genetics, and the study of neural circuits [5]. The most prominent property of the neural system, is its ability to transmit information in terms of electrical signals. Measurements of these electrical signals is a prerequisite of our understanding of the brain, but the measurements are without value if we cannot interpret them. Mathematical modelling have vastly improved our ability to explain the origin and the transmission of the signals. The introduction of computational models have taken it to the next level. We are now able to simulate the overall behaviour of large networks of neurons, as well as making detailed models of individual neurons. To unite the experimental results and the simulations is a never-ending challenge. To meet this challenge, we must be aware of what our models account for, and what they do not account for.

The electrical signals in the brain are made and transported by nerve cells – the neurons. Common to all neurons is the soma, the axon and the arborized dendrites (see the left panel of Figure 1.1). The neuronal membrane separates what is called the intracellular space from the extracellular space, and it is vital to the neurons ability to make and transport electrical signals. The electrical properties of the membrane can be explained by an equivalent circuit (see the right panel of Figure 1.1). There is a voltage difference across the membrane, called the membrane potential. The membrane potential is caused by a difference in charge between the intracellular space and the extracellular space. The difference in charge is represented by the capacitor in the equivalent circuit. Currents, mediated by ions, may flow through channels in the membrane. The most important ion species are sodium and

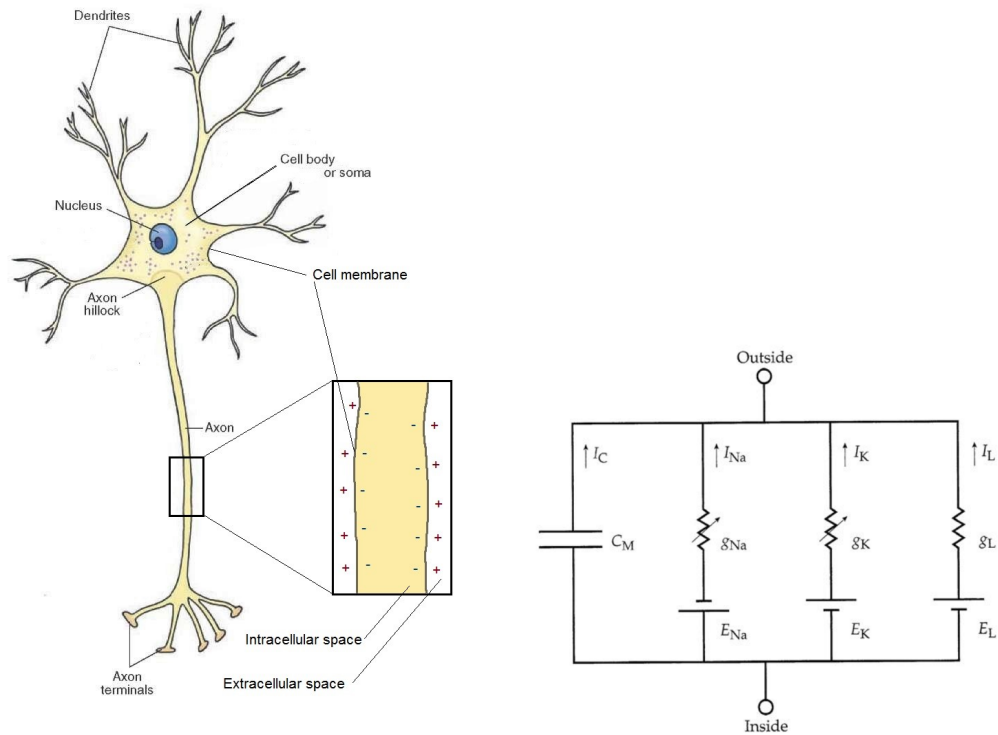


Figure 1.1: Left: A neuron with dendrites, soma, nucleus, axon hillock, axon, and axon terminals. A close-up view of a part of the cell membrane. The cell membrane separates a small negative charge in the intracellular space from a small positive charge in the extracellular space. The charge separation results in a membrane potential. Modified from <http://what-when-how.com/neuroscience> Right: The equivalent circuit of a patch of the neuronal membrane.

potassium. Other ions that cross the membrane are represented by a leak current in Figure 1.1.

A neuron generates signals by letting electrical currents through its membrane, which in turn changes the membrane potential. The change in the membrane potential is accompanied by a change in the potential in the extracellular space. Information about neuronal activity can be obtained by inserting electrodes into the brain, and measuring the electrical potential in the extracellular space. The extracellular potentials are varying with time, and a frequency decomposition of the signal can be useful when it comes to interpreting the signal and identifying connections between the measured signal and the neuronal activity.

The activity of numerous neurons contributes to the extracellular po-

tential, obscuring the contribution of each individual neuron. The so-called volume conductor theory relates transmembrane currents to the potential in the extracellular space. This is a powerful framework, which can be used both for the forward modelling scheme, where transmembrane currents are used to compute extracellular potentials, or for the inverse modelling scheme, where extracellular potentials are used to compute the transmembrane currents [6]. As all models, the volume conductor theory is based on a set of assumptions. One of them, is the assumption that transmembrane currents are the sole cause the extracellular potential, and that other currents, the diffusive, advective and displacement currents, are negligible. The accuracy of the volume conductor theory depends on the validity of this assumption [3].

The transmembrane currents are mediated by ions. Intense neuronal signalling may locally change the ionic composition of the extracellular space, and produce ionic concentration gradients. It is well known that concentration gradients produce a diffusion potential. What is more questionable, is whether this diffusion potential may affect the extracellular potential. If this is the case, what are the circumstances under which the diffusive currents must be included/added to the volume conductor theory? This question has been addressed recently by Halnes et al. [2].

Halnes et al. have simulated the dynamics of a population of neurons and the extracellular space surrounding them. In the simulations, the neurons were active for a long enough time for concentration gradients to be established. They used two models for the dynamics of the extracellular space, one which allowed for diffusion, and one that did not. By comparing the dynamics of the extracellular potential with and without diffusion, they concluded that the diffusive currents had no impact on the fast temporal scale. On the slow temporal scale, however, the diffusive currents induced shifts in the extracellular potentials, and changed the frequency composition of the extracellular potential in the low-frequency range (smaller than 1 Hz).

This project further investigates the nature of the diffusion potential. While the results of Halnes et al. were purely based on simulations of neuronal activity, I used experimentally recorded ionic concentration profiles, found from previously published studies to model the diffusion potential. The modelling of the diffusion potential was done by developing a numerical scheme based on the Kirchoff–Nernst–Planck formalism¹ [1][2]. I have

¹The Kirchoff–Nernst–Planck formalism is to combine the Nernst–Planck equation, an

compared the simulated diffusion potentials to recorded local field potentials from other previously published studies. I found that diffusion potentials were much smaller than the local field potentials – for all frequencies.

Diffusion is a slow process. In the extracellular space, there are many mechanisms which help the concentrations to return to baseline faster than by diffusion only. I have incorporated this in my model by the option of replacing the diffusive decay of the concentration gradients with an exponential decay. I used half-lives from experiments and simulated the diffusion potential. I found that a shorter half-life produced a stronger signal at frequencies near 1 Hz, but that the diffusion potential still was smaller than the recorded extracellular potentials.

Under pathological conditions, the extracellular concentration gradients may become abnormally large. One example is a phenomenon called spreading depression. The phenomenon has received a lot of attention, because it is linked to a number of diseases, including migraine, ischemic stroke, intracranial hemorrhage, and traumatic brain injury [7]. Spreading depression is a slowly propagating wave that precludes the generation and transmission of electrical signals in the brain [7]. During spreading depression, massive rises in the extracellular potassium concentrations have been recorded [7][8]. I have simulated the diffusion potential with ionic concentration profiles recorded during spreading depression, and I found that in this case, the diffusion potential was higher than the recorded extracellular potential for frequencies less than a few Hz. In simulations with exponentially decaying concentration gradients, and half-lives from experiments, I found the diffusion potential to exceed the local field potential. It is possible that diffusion plays a role during spreading depression, and that a better understanding of the diffusion potential may improve our understanding this phenomenon.

This thesis is structured as follows. In the Background section, the relevant background theory and results from previously published studies is presented. The Methods section is devoted to the numerical scheme I have implemented, a discussion of how to use the data from the previous studies, and the strategy I have used to do an error analysis. The Results section contain the error analysis, an evaluation of the model for the initial conditions, as well as the results of the simulations. The Results section also includes an exponential model for the concentration dynamics. The Discussion sec-

ordinary differential equation describing the electrodiffusion of ions in a solution with, Kirchoff's law of current conservation.

tion summarize the main findings regarding the properties of the diffusion potential and its possible contribution to the local field potential.

Chapter 2

Background

2.1 Ionic concentrations and neuronal signalling

2.1.1 The resting membrane potential

The neuronal membrane has an ability to maintain a difference between the extracellular and the intracellular concentrations of specific ions species. The most prominent ion species are listed in Table 2.1. The concentration difference is possible because the membrane is a lipid bilayer, impermeable to ions. The membrane has embedded proteins. Ionic channels and ionic pumps are such proteins. An ionic channel let ions move along their gradient, while ionic pumps use energy in the form of ATP molecules to move ions against their gradient. The work of the ionic pumps maintains a concentration difference between the intracellular and the extracellular space. When the membrane is resting, that is, when it is not involved in any electrical signalling, the channels in the neuronal membrane makes the membrane more permeant to potassium ions than it is to sodium ions. A membrane which separates two solutions, but which is partially permeant to some of the solutes, gives rise to a separation of charge, caused by the diffusion of the permeant ions. The Goldman equation

$$V_m = \frac{RT}{F} \ln \frac{\sum_k z_k P_k [k]_o}{\sum_k z_k P_k [k]_i} \quad (2.1)$$

predicts the voltage across such a membrane, where $V_m \equiv V_i - V_o$ is the voltage difference between the inside and the outside, P_k is the permeability to ion species k , z_k is the valence, $[k]_o$ is the concentration on the outside and $[k]_i$ is the concentration on the inside. R is the gas constant, F is

Faraday's constant and T is the temperature. With the values of Table 2.1 and permeabilities measured in mammalian neuronal membranes, it gives a voltage of approximately -70 mV [5]. This is the resting membrane potential of the neuron.

Table 2.1: The typical values for baseline ionic concentrations of some ion species in mammals [5]. The concentrations vary among different cortical regions and animal species.

ion species	intracellular	extracellular
K ⁺	140 mM	5 mM
Na ⁺	5-15 mM	145 mM
Cl ⁻	4-30 mM	110 mM
Ca ²⁺	0.0001 mM	2 mM

2.1.2 Action potentials

Information is conveyed from one place in the nervous system to another by electrical signals, or action potentials [5]. The ion channels of the neuronal membrane is the key to the generation and transmission of action potentials. Some channels, called voltage-gated channels, open or close depending on the voltage across the membrane. When voltage-gated channels open, the membrane's permeability to a specific ion species increases drastically. If the potential becomes higher than the resting membrane potential, the voltage-gated Na⁺ channels open, and the membrane becomes highly permeable to Na⁺. As Na⁺ flow across the membrane, they take a positive charge with them, making the membrane potential even higher. When the membrane potential is higher than the resting potential, the membrane is said to be depolarized. If the depolarization reaches a certain threshold, an action potential is generated. The high membrane potential opens the voltage-gated K⁺ channels, and it closes the voltage-gated Na⁺ channels. K⁺ rush out of the cell, and the membrane potential returns quickly to its resting level. A consequence of this generation of an action potential is a transient Na⁺ influx and K⁺ efflux to the cell. Because the action potential is most often generated in the axon hillock [9], these ionic fluxes are largest in the soma region (see Figure 1.1).

Normally, the Na⁺ flux into the cell and K⁺ out of the cell are considered so small that they do not change the baseline concentrations of table 2.1.

Still, experiments [10][11][4] have shown that intense neuronal firing of action potentials produce deviations from the baseline concentrations. In Section 2.7 results from some selected experiments are presented.

2.1.3 Deviation from electroneutrality

The resting membrane potential and the generation of action potentials rely on a separation of charge, and thereby a local deviation from electroneutrality. In a system with deviation from electroneutrality, there will be electrical forces trying to even out the charge accumulation. The separation of charge requires energy, which has a fundamental consequence. In a model of the movement of ions, if we cannot account for the energy needed to separate charges, we must assume the system to behaves in an electroneutral way, that is, at every point in space the movement of an ion must be accompanied of the movement of another ion, so that the net charge going into or out of the point is zero. This can be done in two ways: the a cation moves together with an anion, or a cation is exchanged by another cation. I will use the assumption of electroneutrality in the making of the model for the diffusion potential.

2.1.4 Intercellular signalling

In the brain, the neurons are interconnected in large networks. One neuron may receive input, or stimuli, from thousands of other neurons. The neuron receives input to its dendrites. Electrical signals travels from the dendrites to the soma. Depending on the amount of stimuli, the neuron may respond by generating an action potential. The action potential travels down the axon. The axon branches to axon terminals. The axon terminals are connected to the dendrites of other neurons by synapses.

2.2 Layered structures in the brain

The cerebral cortex is the largest part of the mammalian brain. It is has a sheetlike structure. The surface area and the thickness of the cortex depends on the animal species. In humans it has a area of 0.24 m^2 , and a thickness of $2.3 - 2.8 \text{ mm}$ [12]. The cortex is confined to the volume of the skull, in humans and other large mammals, the sheet is folded, giving the brain

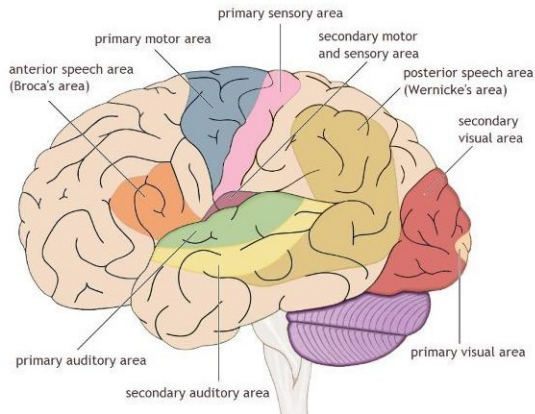


Figure 2.1: Left: Spongebob with his brain exposed, featuring the folded sheet-like structure of the cortex (<http://spongebob.wikia.com>). Right: a schematic drawing of the human cortex (beige) and its functional areas (colored). Cerebellum in purple (https://my-ms.org/anatomy_brain_part1.htm)

the characteristic appearance we recognize from the popular culture and textbooks, as illustrated in Figure 2.1. The cortex has a laminar organization, the largest part of the cortex, neocortex, has six layers. Each cortical layer has a primary source of inputs a primary source of targets [5], and each layer is occupied with some specific types of neurons, see Figure 2.2. For example, the internal pyramidal layer is mainly occupied with large pyramidal neurons with their axons travelling down, while the internal granular layer contains different types of stellate and pyramidal neurons.

The cortex is also divided into functional areas that serve various sensory, motor, and cognitive functions (as illustrated in the right panel of Figure 2.1). As a consequence, one particular input, can give stimuli to one particular type of neurons in a particular layer, making a response that vary across the cortical depth, but is the same within this layer. For example, the stellate neurons in layer IV of the primary visual area may receive an input signal caused by a visual stimuli. The stellate neurons convey the signals to the pyramidal cells in layer V. The pyramidal cells generate action potentials, which travel down their axons. This process leaves a signature in the extracellular space in terms of a change in the extracellular potential and possibly in the ionic concentrations. The signature is unique for each layer, but more or less the same within the layer [5]. This characteristic encourages measurements of laminar profiles of the extracellular potentials and ionic concentration gradients, and serves as an argument for using a one

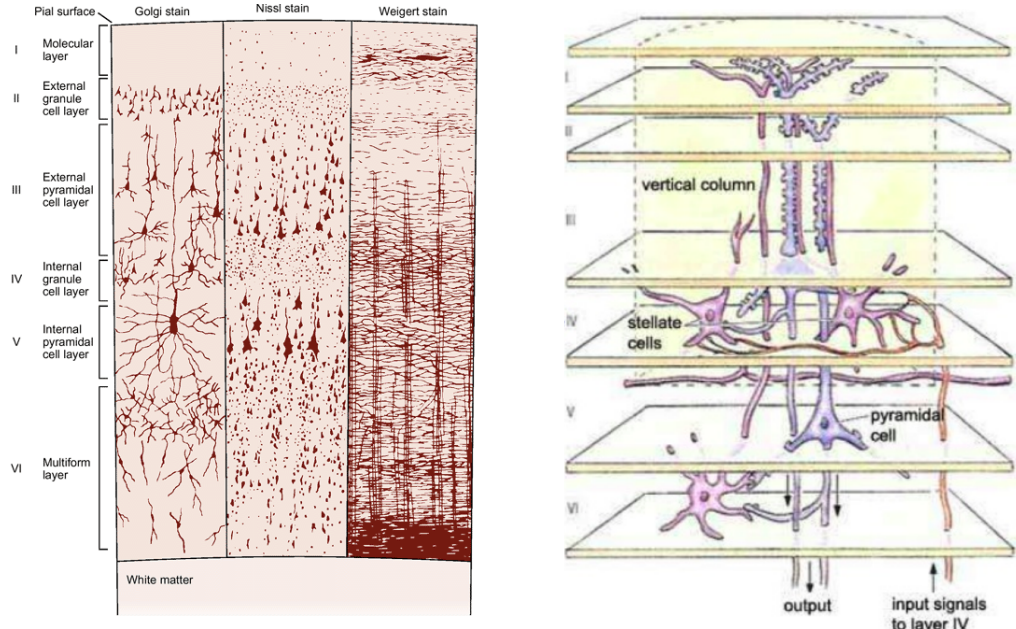


Figure 2.2: Left: The laminar organisation of neocortex, as it appears with different staining methods (<https://www.quora.com>). Right: Input signals to stellate neurons in layer IV is conveyed to the pyramidal cells in layer V, where new action potentials are generated (<http://slideplayer.com/slide/8215330/>).

dimensional model for the extracellular dynamics [13].

2.3 Local Field Potentials

The generation of action potentials and the conveying of electrical signals in the neurons shift the membrane potential, V_m , with the help of transmembrane currents. Electrical currents into and out of the extracellular space affect the extracellular potential, Φ . Extracellular potentials are measured by inserting an electrode into the brain and comparing the potential to the potential at a reference point, V_∞ . Typical electrodes in modern day experiments have many recording sites which have a distance of 0.1 mm [14] between them, and gives a laminar profile of the extracellular potential.

Action potential generation involves fast potential dynamics, and this activity is visible in the high frequency part of the potential, the Multi Unit Activity (MUA). High-frequency signals are damped rapidly, for this reason the MUA is said to contain information about the firing of action potentials of a handful of the surrounding neurons.

The Local Field Potential (LFP) is defined as the low-frequency part of the extracellular potential. In contrast to the MUA, the LFP appears to predominantly reflect the synaptic inputs to the neurons, and it may reflect activity from thousands of neurons located in its vicinity [14].

The interpretation of the signal in terms of the underlying neural activity is not straightforward. The problem of predicting transmembrane currents from electrode measurements is called current Current Source Density (CSD). CSD analysis of multiple LFP recordings across well-organized layered neural structures such as cortex, cerebellum, and hippocampus allows for a more local measure of neural activity than the LFP, which is easier to interpret in terms of the activity in the underlying neural circuits [14]. For CSD analysis, an inverse modelling scheme is used. The density of the (neuronal) current sources is computed from the LFP, in the framework of the volume conductor theory [15].

2.4 The Nernst–Planck equation

Diffusion is a process caused by the random walk of particles when a concentration gradient is present. There will be a particle flux towards lower concentration. The flux is determined by the concentration gradient, but also by the diffusion coefficient of the particles. A high diffusion coefficient will even out the concentration gradient more rapidly. The concentration dynamics for a purely diffusive process is given by Fick’s law:

$$\mathbf{J}_{\text{diff},k} = -\mathcal{D}_k \nabla c_k \quad (2.2)$$

Where $\mathbf{J}_{\text{diff},k}$ is the particle flux of ion species k , \mathcal{D}_k is the diffusion coefficient and c_k is the concentration.

Electric migration is the process where electrically charged particles moves towards a lower potential. The flux is determined by the potential gradient, $\nabla\Phi$, and the valence of the ions, z_k .

$$\mathbf{J}_{\text{field},k} = -\frac{\mathcal{D}_k z_k F}{RT} c_k \nabla\Phi \quad (2.3)$$

The temperature T is considered constant, F is Faradays constant and R is the gas constant. In extracellular space, the effective diffusion coefficient $\mathcal{D}_k = D_k/\lambda_n^2$ is composed of the diffusion coefficient D_k in dilute solutions,

and the tortuosity factor λ_n , which summarizes the hindrance imposed by cellular structures [16]. Combine diffusion and electric migration, and we have:

$$\mathbf{J}_k = -\frac{D_k}{\lambda_n^2} \nabla c_k - \frac{D_k z_k}{\lambda_n^2 \Psi} c_k \nabla \Phi \quad (2.4)$$

where $\Psi \equiv RT/F$. The flux of ion species k is related to the change in concentration by the continuity equation.

$$\frac{\partial c_k}{\partial t} = -\nabla \cdot \mathbf{J}_k \quad (2.5)$$

which leads to the Nernst–Planck equation, a partial differential equation describing the relation between the change in concentration, the concentration gradient and the potential gradient:

$$\frac{\partial c_k}{\partial t} = \frac{D_k}{\lambda_n^2} \nabla^2 c_k + \frac{D_k z_k}{\lambda_n^2 \Psi} \nabla \cdot (c_k \nabla \Phi) \quad (2.6)$$

2.5 The diffusion potential

Electrodiffusion is, in general, a process where ionic movement can be described by equation 2.6. The diffusion potential (as it will be referred to here) is an electric potential caused by concentration gradients of ion species with different diffusion coefficients. In this section, a thought experiment is used to illustrate this effect. Consider a solution with equal amounts of Na^+ and Cl^- , prepared so that initially the concentration c of both ion species is a step function

$$c(x, t=0) = \begin{cases} c_1^0 & \text{for } x \leq 0 \\ c_2^0 & \text{for } x > 0 \end{cases} \quad (2.7)$$

where $c_1^0 < c_2^0$. Then there is a gradient in $[\text{Na}^+]$ and $[\text{Cl}^-]$, and the concentrations will change with time to even out the difference. The concentration dynamics is described by two effects:

1. The Cl^- concentration even out faster because Cl^- has a larger diffusion coefficient.
2. If there is an electrical field, it will affect Na^+ and Cl^- in opposite ways, because they have opposite charge.

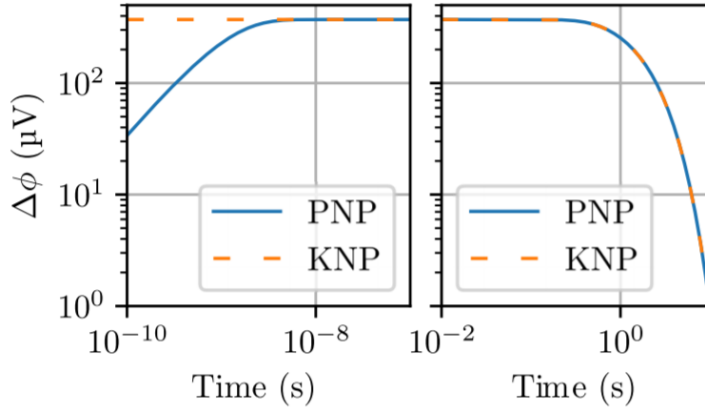


Figure 2.3: The simulated dynamics of the diffusion potential. The blue line with legend PNP represents the potential of a system which allows for deviation from electroneutrality, while the orange line represents a system where the diffusion potential is assumed to be established immediately, and the system is electroneutral for all times. After 10 ns, the lines overlap. This indicates that a quasi-stationary state is reached, and the assumption of electroneutrality is valid [15].

In the beginning, there is no electrical field. Cl^- diffuses faster than Na^+ , leaving a small positive charge in the region $x \leq 0$, and taking a small negative charge to the region $x > 0$. When there is a difference in charge between the two regions, there is also an electrical field. The emerging electrical field slows down the Cl^- , and speeds up the Na^+ . Because the field is created by the faster Cl^- , the field will increase slower and slower as the diffusion speed of the two ions become more equal. When the diffusion speeds are equal, there is no longer a net movement of charge. Then, the electrical field is just large enough to keep the Cl^- flux equal to the Na^+ flux, and the field has reached a quasi-stationary state. Solbrå et al. [15] have simulated the dynamics of the diffusion potential, which is the blue line with legend PNP in Figure 2.3.

As illustrated in the left panel of Figure 2.3, the quasi-stationary state is established within the first 10 ns. The orange dashed line with legend KNP correspond to a system which at every time is electroneutral. That is, apart from the small charge separation required for the diffusion potential, every point in space has zero net charge.

$$\sum_k z_k c_k = 0$$

The electroneutrality assumption will be an underlying assumption for the following, even though it is not strictly true. It represents a quasi-stationary solution of equation 2.6, but the diffusion potential is decaying with time as the concentration gradients flattens out. In the simulation by Solbrå et al., this process starts after approximately 1 s, as illustrated in the right subpanel of figure 2.3.

The origin of the diffusion potential is the difference in the diffusion coefficient of the two ion species. If there were no difference, the ion species would diffuse with the exact same speed, all the time. Then, there would be no separation of charge to produce an electrical field. In the two-ion system described above, the ions move with the same speed after the diffusion potential has been established.

In section 2.10.1 I show that it is possible to find an effective diffusion coefficient so that the system can be described by the diffusion equation alone. The diffusion equation has analytical solutions. I have incorporated a solution of the diffusion equation in my thesis, because it makes me able to do an error analysis on the numerical scheme which I have used to solve equation 2.6. The analytical solution is presented in section 2.10.2, and the error analysis is in section 4.1.

2.6 Electrodiffusion in the extracellular space

The process of electrodiffusion in the extracellular space can modelled by solving the Nernst–Planck equation with initial conditions from previously published experiments. In Section 2.2, I argue that due to the laminar structure of many brain regions, variations in relevant extracellular variables occur in only one spatial dimension. Thus, the electrodiffusion in the extracellular space can be reduced to a one-dimensional problem, where the concentrations and the potential is a function of the cortical depth x . In one dimension, the Nernst–Planck equation (equation 2.6) takes the form

$$\frac{\partial c_k}{\partial t} = \frac{D_k}{\lambda_n^2} \frac{\partial^2 c_k}{\partial x^2} + \frac{D_k z_k}{\lambda_n^2 \Psi} \frac{\partial}{\partial x} \left(c_k \frac{\partial \Phi}{\partial x} \right) \quad (2.8)$$

Solving equation 2.8 involves two solutions: $\Phi(x, t)$ and $c_k(x, t)$. This calls for one more relation between Φ and c_k . The Kirchoff–Nernst–Planck formalism [16] [2] combines the Nernst–Planck equation and Kirchoff’s law for current

conservation. The net current I is the sum of all the ion fluxes:

$$I = \sum_k z_k F J_k = -\frac{F}{\lambda_n} \sum_k z_k D_k \frac{\partial c_k}{\partial x} - \frac{F}{\lambda_n \Psi} \sum_k z_k^2 D_k c_k \frac{\partial \Phi}{\partial x} \quad (2.9)$$

In simulations of the extracellular potential where neurons are included, these are represented as current sinks and current sources. In a system where there are no active neurons, there cannot be any current sinks or sources, if not there would be an accumulation of charge. For an isolated system, $I = 0$ is a requirement. Because the potential Φ is equal for all ion species, equation 2.9 gives an expression for $\frac{\partial}{\partial x} \Phi$:

$$\frac{\partial}{\partial x} \Phi = \frac{-\Psi \sum_k z_k D_k \frac{\partial}{\partial x} c_k}{\sum_k z_k^2 D_k c_k} \quad (2.10)$$

Equation 2.10 can be inserted into Equation 2.8 to find $c_k(x, t)$, and it can be integrated to find the diffusion potential itself. The boundaries are chosen so that the extracellular potential Φ is the difference between the potential V_o and the potential at some reference point V_∞ . The main focus of this work is on the diffusion potential Φ , but the solution $c_k(x, t)$ is useful for comparing the numerical solution to an analytical one.

2.7 Previously published extracellular concentration recordings

2.7.1 Laminar concentration profiles

Deviations from baseline concentrations in the extracellular space is the origin of the extracellular diffusion potential. In Figure 2.4, a selection of laminar concentration profiles is presented. The concentration profiles are taken from previously published studies.

Figure 2.4, upper left subpanel, is taken from Dietzel et al. [10] and show recordings of Na^+ and Ca^{2+} from the sensimotor cortex of cats, due to stimulation at all cortical depths (0.1 mm spacing between). In this experiment, the electrodes used for recording Na^+ were also sensitive to Ca^{2+} . This was corrected for, and the data points marked as $[\text{Na}^+, \text{Ca}^{2+}]$ are the corrected values of the $[\text{Na}^+]$. In this experiment, there was a decrease of extracellular Na^+ in all cortical layers. The extracellular Ca^{2+} showed a decrease in

the upper cortical layers, but an increase in the lower layers. $\Delta[\text{Ca}^{2+}]$ is a magnitude of 10 lower than $\Delta[\text{Na}^+]$.

Figure 2.4, lower left subpanel, is taken from Nicholson et al. [11] and shows recordings of K^+ and Ca^{2+} in the cerebellar cortex of cats, due to surface stimulation. A stimulation frequency of 20 Hz gave the largest $\Delta[\text{K}^+]$ and the largest $\Delta[\text{Ca}^{2+}]$. $\Delta[\text{Ca}^{2+}]$ is a magnitude of 10 lower than $\Delta[\text{K}^+]$.

Figure 2.4, upper right subpanel, is made with data from the simulations of Halnes et al. [2]. Halnes et al. have simulated a network of 10 pyramidal neurons, and kept track of the ionic output. In figure 2.4 is the concentration profiles at a selected time point in the simulation.

Figure 2.4, lower right subpanel, is taken from Coldingley & Somjen [4] and shows recordings of K^+ in the visual cortex of cats, due to surface stimulation and stimulation at a deeper cortical layer.

2.7.2 Concentrations of the other ion species

Dietzel et al. [10] have done simultaneous measurements of Na^+ and Ca^{2+} as presented in the previous section, but also of Na^+ and K^+ , and of Na^+ and Cl^- . In these experiments, the focus was on the kinetics of the concentrations, rather than the laminar profile. In their experiments, they found that the changes in $[\text{Cl}^-]$ were slow, and often not observable during the stimulation period. Simultaneous measurements of $[\text{K}^+]$ and $[\text{Na}^+]$ at a depth of 1000 μm revealed that the increase in K^+ had the same time course as the decrease in Na^+ for the first 10 s. At higher cortical levels, there was a fast Ca^{2+} decrease which inferred with the measurements, but when this were corrected for they found reason to believe that there was a 1:1 Na^+/K^+ exchange at all cortical levels during the stimulation period.

2.7.3 The time course of the $[\text{K}^+]$ decay

Cordingley & Somjen [4] studied the half-life for the $\Delta[\text{K}^+]$, and found it to be $\sim 1 - 3$ s. They also calculated the theoretical half decay for a diffusive process, and found this half-life to be 178 s. Their conclusion was that all or most of the K^+ lost from neurons during activity is pumped back so fast that it has no chance to move away by diffusion. Dietzel et al. [10] have also studied the dynamics of K^+ after the stimulation was ended. They found the half-life of $\Delta[\text{K}^+]$ to be somewhat larger, approximately $\sim 5 - 10$ s. The

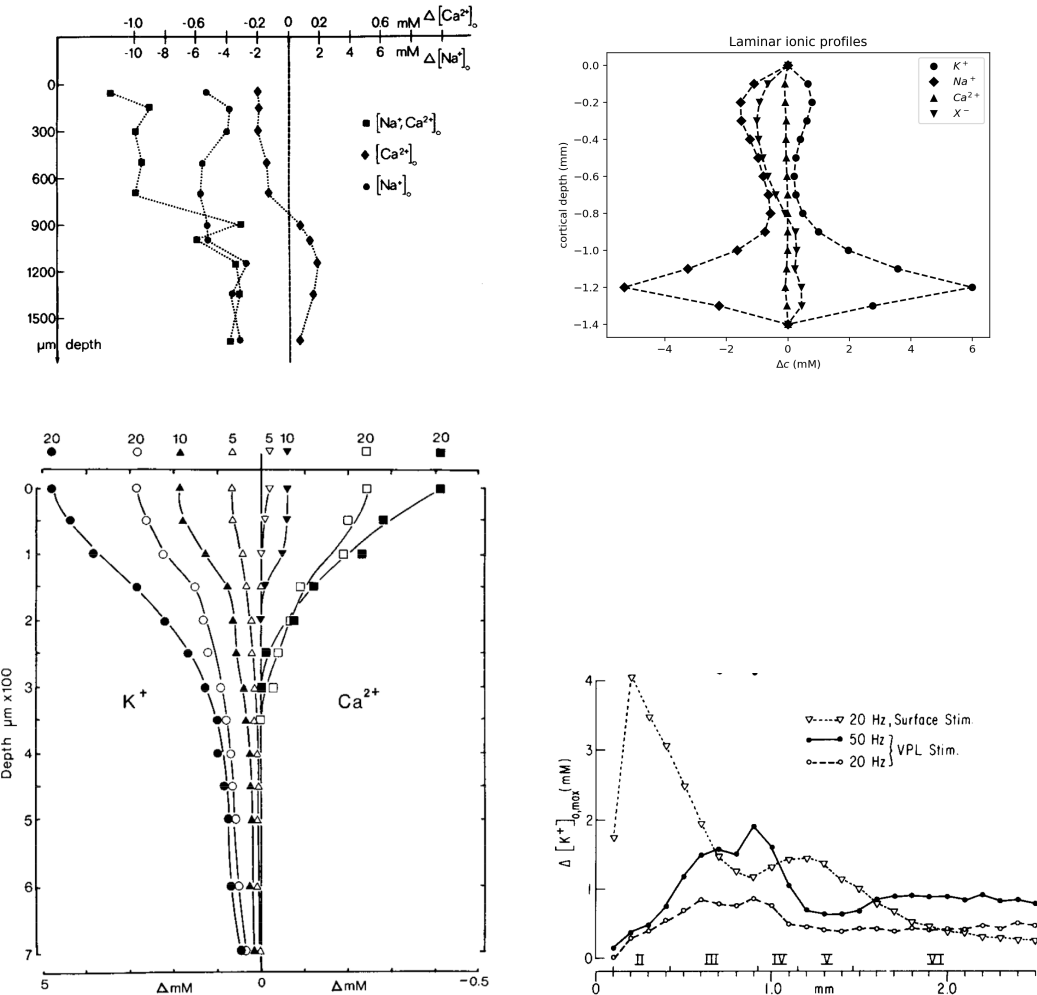


Figure 2.4: Previously published extracellular concentration recordings. Upper left: Na^+ and Ca^{2+} profile recorded from sensimotor cortex of cats by Dietzel et al. Stimulation: 15-20 Hz for 10 s. Lower left: K^+ and Ca^{2+} recorded from cerebellar cortex of cats by Nicholson et al. Frequencies associated with profiles marked on upper abscissa. Stimulation time is 30 s. Maximum deviation from baseline was reached after 10 s, solid dots and squares/the outer curves. Upper right: ionic output simulated by Hahn et al., using 10 pyramidal neurons. Lower right: K^+ recorded from visual cortex of cats by Cordingley and Somejen. Stimulation time was 1 s. Both surface stimulation and VPL stimulation (stimulation of the estimated cortical depth of the neuronal nuclei).

maximum concentration deviation in this case was 6 mM, which is more than what was found by Cordingley & Somjen [4].

2.8 The power spectrum density

The diffusion potential is varying slowly with time, and its contribution to the local field potential is in the lowest frequencies [2]. Comparison of the frequency components of the signal is achieved with the help of the Power Spectrum Density (PSD), a concept from signal analysis. It is a representation of the frequency components of a signal. The PSD is obtained with the help of the Fourier transform, which is a transform from the time domain to the frequency domain, defined as

$$\mathcal{F}(f) = \int_{-\infty}^{\infty} v(t)e^{-i2\pi t f} dt \quad (2.11)$$

where $v(t)$ is the original time-dependent signal, and $\mathcal{F}(f)$ is the Fourier transform, which is a function of the frequency f . The frequency components are the signal's amplitude at this frequency. When the signal is discrete, the Fast Fourier Transform (FFT) algorithm can be used for calculating the Fourier transform [17]. The PSD is obtained by: normalizing the FFT by dividing by its length, the sampling frequency f_s ; find the absolute value of the FFT; squaring the FFT; and discarding upper half of the frequencies and multiplying by two [18]. The procedure is summed up in the following equation.

$$\text{PSD} = 2 \left(\frac{|\mathcal{F}(f)|}{f_s} \right)^2 \quad f \in (0, \frac{f_s}{2}) \quad (2.12)$$

Figure 2.5 illustrates how the PSD is a representation of the frequency component. In the left panel, a superposition of three sine waves,

$$v(t) = \sin(2\pi t) + 0.4 \sin(8\pi t) + 0.1 \sin(64\pi t)$$

is shown. The PSD of the signal is in the right panel. The frequencies of the signal are 1, 4 and 32 (in arbitrary units), and the same frequencies are represented in the PSD. The signal component with the largest amplitude, gives the largest power at this frequency.

In experiments where the local field potential is measured, the measurements are often presented as PSDs, because this representation makes it possible to spot the dominating frequencies of the signal. In many publications, the PSD is presented in arbitrary units, which makes it hard to relate the PSD to the magnitude of the original signal.

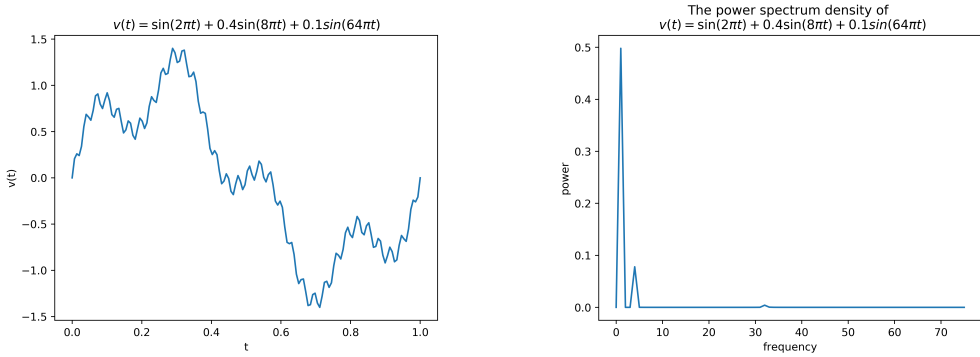


Figure 2.5: Left: A signal composed of sine waves with frequencies 1, 4 and 32 (in arbitrary units). Right: The PSD of the signal. The frequencies of the signal (1, 4 and 32) are peaks in the PSD.

2.9 Spreading depression

The concentration gradients and the concentration dynamics presented in section 3.3 are due to intense, but still not abnormal neural activity. A phenomenon where much larger concentration gradients are observed and where diffusion is believed to play a role, is spreading depression. Spreading depression is a slowly propagating wave of intense but transient regional depolarization of neurons (and glia and perhaps all cells) [7]. Spreading depression is a positive feedback loop, of which I will here try to give a rough outline. A sudden opening of nonselective large-conductance cation channels lets Na^+ flow into the neuron, and K^+ flow out. This results in a depolarization of the neuronal membrane (according to the Goldman equation), together with a drop in the extracellular potential. The membrane potential $V_m = V_i - V_o$ is related to the extracellular potential Φ by $\Phi = V_o - V_\infty$, where V_∞ is the potential at some reference point.

The extracellular K^+ clearance mechanisms become overloaded, and massive K^+ efflux raises $[\text{K}^+]$ from $\sim 3 \text{ mM}$ at resting state to over $30 - 50 \text{ mM}$, and sometimes as high as 80 mM . The massive rise in K^+ is sufficient to depolarize the neighbouring cells and is the critical factor mediating the contiguous spread of the wave [7]. The drop in the extracellular potential is only partly accounted for by the depolarization of the membrane. It is speculated that a diffusion potential might contribute [8].

Because spreading depression is associated with extremely high, but transient, extracellular K^+ concentrations, we can expect large concentration

gradients as well. It is possible that concentration gradients of this scale results in a diffusion potential that has a substantial impact on the LFP. During spreading depression the neuronal dynamics differs from the dynamics described in section 3.3, because other channels than the ordinary voltage gates are open. The concentration shifts are approximately

$$\Delta[\text{Na}^+] = -2\Delta[\text{K}^+] \quad \Delta[\text{Cl}^-] = -\Delta[\text{K}^+]$$

The value of $\Delta[\text{K}^+]$ depends on the baseline concentration [8] [7]. The half-life is approximately 30 s [7].

2.10 An analytical solution of a simplified system

2.10.1 The effective diffusion coefficient of a two-ion system

Consider a system with two ion species 1 and 2 where $z_1 = -z_2$ and the diffusion coefficients are D_1 and D_2 . The system is prepared so that the concentrations are equal: $c_1 = c_2 = c$, but not homogeneous. In bulk, the ions must diffuse with the same speed to maintain electroneutrality. To make this happen, an electrical field which slows down the fastest ion and speeds up the slowest one, emerge. I want to find the joint diffusion coefficient D , that is, the diffusion coefficient the ions both should have had in order to diffuse with this speed without the presence of a field. In other words, I want to find D so that it satisfies:

$$D_1 \frac{\partial c}{\partial x} + \frac{D_1 c}{\Psi} \frac{\partial \Phi}{\partial x} = D \frac{\partial c}{\partial x} \quad (2.13)$$

$$D = D_1 + D_1 \frac{c}{\Psi} \frac{\frac{\partial \Phi}{\partial x}}{\frac{\partial c}{\partial x}} \quad (2.14)$$

The zero current requirement gives :

$$D_1 \frac{\partial c}{\partial x} + \frac{D_1 c}{\Psi} \frac{\partial \Phi}{\partial x} - D_2 \frac{\partial c}{\partial x} + \frac{D_2 c}{\Psi} \frac{\partial \Phi}{\partial x} = 0 \quad (2.15)$$

Rearrange it so that left hand side is expressed in terms of D_1 and D_2 :

$$\frac{D_2 - D_1}{D_1 + D_2} = \frac{c \frac{\partial \Phi}{\partial x}}{\Psi \frac{\partial c}{\partial x}} \quad (2.16)$$

Inserted into 2.14:

$$D = D_1 + D_1 \frac{D_2 - D_1}{D_1 + D_2} = \frac{D_1(D_1 + D_2) + D_1(D_2 - D_1)}{D_1 + D_2} = \frac{2D_1D_2}{D_1 + D_2} \quad (2.17)$$

The two ions with opposite valence and diffusion coefficients D_1 and D_2 will in the presence of the diffusion potential move in the same way as two ions with the same diffusion coefficient D , not subjected to a potential.

2.10.2 The analytical solution to the one dimensional diffusion equation

The diffusion equation is Fick's law (Equation 2.2) inserted into the continuity equation (Equation 2.5):

$$\frac{\partial c}{\partial t} = D \nabla^2 c \quad (2.18)$$

The diffusion equation has analytical solutions. Here is a solution of the one-dimensional diffusion equation

$$\frac{\partial c}{\partial t} = D \frac{\partial^2 c}{\partial x^2} \quad (2.19)$$

for homogeneous boundary conditions,

$$c(0, t) = c(L, t) = 0 \quad t > 0$$

where L is the length of the system. The separation of variables technique gives

$$c(x, t) = X(x)T(t)$$

$$\frac{\partial c}{\partial t} = T'X$$

$$\frac{\partial^2 c}{\partial x^2} = TX''$$

Inserted into the equation 2.19

$$T'X = DTX'' \implies \frac{T'}{DT} = \frac{X''}{X} = \text{constant}$$

Let the constant be $-\lambda^2$. We then have two separate equations:

$$T' + \lambda^2 T = 0 \implies T = e^{-\lambda^2 t D}$$

$$X'' + \lambda^2 X = 0 \implies X = A \sin \lambda x + B \cos \lambda x$$

The boundary condition $c(0, t) = 0$ requires $B = 0$, while the boundary condition $c(L, t) = 0$ requires that λ is a multiple of π : $\lambda_k = k\pi/L$, where $k = 1, 2, 3, \dots$. We now have the solution $c(x, t) = X(x)T(t)$

$$c(x, t) = \sum_k A_k \sin \frac{k\pi x}{L} \cdot e^{-Dk^2\pi^2 t/L^2} \quad (2.20)$$

where A_k are the Fourier coefficients of the initial concentration. The simplest initial condition is:

$$c(x, 0) = c_0 + \Delta c_{\max} \sin \frac{\pi x}{L}$$

Then, there is no need for a Fourier expansion, as $k = 1$ and $A_1 = \Delta c_{\max}$ satisfies 2.20, and the solution is

$$c(x, t) = c_0 + \Delta c_{\max} \sin \frac{\pi x}{L} \cdot e^{-D\pi^2 t/L^2} \quad (2.21)$$

In this case, the initial concentration deviation is exponentially decaying for all x , with the time constant $\tau = L^2/(D\pi^2)$. The half-life is $\tau \ln 2$.

Chapter 3

Methods

In this project I have simulated the diffusion potential by finding a numerical solution to the Nernst–Planck equation. I have used the KNP formalism and assumed that there are no neuronal sinks or sources. The assumption of electroneutrality is a prerequisite. This means that the diffusion potential is assumed to be established immediately. For the boundaries of the system, I have used baseline concentrations, and zero potential. This implies that ions are allowed to leak out or into the system, as long as the net current is zero. The constants used in this project are listed in Table 3.1.

Table 3.1: List of constants [2].

symbol	explanation	Value
D_{Na}	Na^+ diffusion coefficient	$1.33 \cdot 10^{-9} \text{ m}^2/\text{s}$
D_K	K^+ diffusion coefficient	$1.96 \cdot 10^{-9} \text{ m}^2/\text{s}$
D_{Cl}	Cl^- diffusion coefficient	$2.03 \cdot 10^{-9} \text{ m}^2/\text{s}$
D_{Ca}	Ca^{2+} diffusion coefficient	$0.77 \cdot 10^{-9} \text{ m}^2/\text{s}$
λ_n	tortuosity	1.6
F	Faraday's constant	96485.333 C/mol
R	Gas constant	8.3144598 J/mol K
T	temperature (considered constant)	310 K

3.1 Numerical scheme for solving the 1D Nernst–Planck equation

There is no analytical solution of equation 2.8, and we must use a numerical solution. The numerical solution involves the discretization of c_k . To

simplify the notation, I skip the index k for the ion species. Then the ionic concentration expressed with the discretized variables $x_i = x_0 + i\Delta x$ and $t_j = t_0 + j\Delta t$ is

$$c_i^j = c(x_i, t_j)$$

For the approximation of the derivatives, there are many schemes to choose from. The straight-forward way is to use the Euler Forward approximation for the time derivative of c_k .

$$\frac{\partial c}{\partial t} \approx \frac{c^{j+1} - c^j}{\Delta t}$$

Then, the current state is used to find the state at the next time step, which means that I for every time step can calculate the value of the right-hand side of equation 2.8, and add it to the current solution.

To make every part of the system electroneutral, it is important that the derivatives on the right-hand side use the same integration points. I found that this is the case with the following approximations for the spatial derivatives.

$$\frac{\partial^2 c}{\partial x^2} \approx \frac{c_{i+1} - 2c_i + c_{i-1}}{(\Delta x)^2}$$

And

$$\frac{\partial}{\partial x} \left(c \frac{\partial \Phi}{\partial x} \right) \approx \frac{1}{\Delta x} \left(c_{i+1/2} \left(\frac{\partial \Phi}{\partial x} \right)_{i+1/2} - c_{i-1/2} \left(\frac{\partial \Phi}{\partial x} \right)_{i-1/2} \right)$$

where

$$c_{i+1/2} = \frac{c_{i+1} + c_i}{2}$$

and by using a central- half point discretization of equation 5

$$\left(\frac{\partial \Phi}{\partial x} \right)_{i+1/2} = \frac{-\Psi \sum_k z_k D_k (\frac{\partial c}{\partial x})_{k,i+1/2}}{\sum_k z_k^2 D_k c_{k,i+1/2}} = \frac{-\Psi \sum_k z_k D_k (c_{k,i+1} - c_{k,i}) / \Delta x}{\sum_k z_k^2 D_k (c_{k,i+1} + c_{k,i}) / 2} \quad (3.1)$$

Now, we have a discretization of equation 2.8 where c^{j+1} is totally determined by c^j and Φ^j (an explicit scheme), and where the same integration points, c_{i-1} , c_i , c_{i+1} are used for both spatial derivatives. The local approximation error of the scheme is $\mathcal{O}(\Delta t)$ and $\mathcal{O}(\Delta x)^2$. A possible risk of using this explicit scheme, is that is unstable if Δx is too small compared to Δt . The stability criterion of the explicit scheme for the diffusion equation is $\frac{D\Delta t}{(\Delta x)^2} \leq \frac{1}{2}$ [19].

I have chosen to work with dimensionless variables. With

$$\Phi = \Psi\Phi' = RT/F\Phi' = 0.0267V\Phi'$$

and

$$\alpha_k = \frac{\Delta t D_k}{(\Delta x)^2 \lambda_n^2}$$

the concentration of ion species k at time t_{j+1} is:

$$c_i^{j+1} = c_i^j + \alpha(c_{i+1}^j - 2c_i^j + c_{i-1}^j) + \alpha z \Delta x \left(\frac{c_{i+1}^j + c_i^j}{2} \left(\frac{\partial \Phi'}{\partial x} \right)_{i+1/2}^j - \frac{c_i^j + c_{i-1}^j}{2} \left(\frac{\partial \Phi'}{\partial x} \right)_{i+1/2}^j \right) \quad (3.2)$$

The solution found by this method, is $c(x, t)$. The potential $\Phi(x, t)$ is the desired solution. I have used the trapezoid rule to integrate $v(x) = \partial \Phi / \partial x$ in an iterative fashion.

$$\int_x^{x+\Delta x} v(x') dx' \approx \Delta x (v(x + \Delta x) + v(x)) / 2 \quad (3.3)$$

3.2 Implementation of the numerical scheme

The solver `solveEquation(Ions, lambda_n, N_t, delta_t, N, delta_x)` was implemented in Python¹. `Ions` is a list containing instances of the class `Ion`. The attributes of an `Ion` ion are three concentration vectors: one that store the initial concentration profile of the ion (`c_init`), one for temporary storing newly calculated concentration profile (`c_new`), and one which is the ion concentration profile at that time step (`c`). The concentration `c` is used to calculate the potential gradient `grad_phi`, according to equation 3.1. `grad_phi` is calculated at the half-points. This means that the `grad_phi` is one element shorter than `c`. `grad_phi`, together with `c`, is used to calculate `c_new`. `solveEquation` calls the function `integrate(v, xmin, xmax)`, which integrates `grad_phi`. The scheme used is the trapezoid rule, where the boundaries are zero at both sides. `integrate` returns the integrated vector for the interior points (edges not included). The integrated vector `Phi` is stored in an array, which is returned by the function `solveEquation`. `Phi` is

¹in the program `electrodiffusion.py` in my github repository, <https://github.com/sigrivi/electrodiffusion>

then a dimensionless quantity, and must be multiplied by Ψ . Equation 3.2 is scaled so that any unit will work for the concentrations, but I have chosen to work with SI units.

3.3 Initial concentration profiles based on recorded ionic concentrations

The laminar profiles of section 2.7 do not have more than two simultaneously measured ion species. This calls for assumptions about the other ion species. Primarily it must be decided how many ion species should be included. Na^+ and K^+ are the ion species which experience the largest concentration shifts, because these ions are the key ions in the generation of the action potentials. Cl^- is the most abundant anion in the extracellular space, and it is necessary in order to make an electroneutral bulk solution. Ca^{2+} is an important signalling ion, and its relative concentration variations are large, but the concentration variations are approximately a tenth of the Na^+ and K^+ variations (see Figure 2.4, left panels). Not all the data sets contain information about Ca^{2+} . Due to the insufficient data set and the small scale of the concentrations, I have neglected Ca^{2+} .

The model requires the initial profiles of Na^+ , K^+ and Cl^- ($[\text{Na}^+]^0$, $[\text{K}^+]^0$ and $[\text{Cl}^-]^0$), while the data sets either are laminar profiles of K^+ or Na^+ . I have tested four possible scenarios for the initial ion composition based on a known $[\text{K}^+]^0$. The scenarios are listed in the following, together with a 5th scenario based on the recordings of a hypothetical experiment where both $[\text{K}^+]^0$ and $[\text{Na}^+]^0$ are known.

Scenario 1: During the generation of action potentials, Na^+ leaves the extracellular space, and K^+ enters. In scenario 1, I have assumed that $\Delta[\text{K}^+]^0 + \Delta[\text{Na}^+]^0 = 0$ to make a depth profile for Na^+ . An implicit assumption is that Cl^- is at baseline initially, and that Na^+ and K^+ are the sole contributors to the diffusive currents. This assumption finds support in the work of Dietzel et al. [10] where simultaneous measurements of K^+ and Na^+ during the stimulation period, indicated that there was a 1:1 Na^+/K^+ exchange in all cortical layers. This was further backed up by measurements of $[\text{Cl}^-]$. The dynamics of Cl^- were slower, the increase in Cl^- was firstly observed after the stimulation

period. Then it makes sense using baseline Cl^- as an initial Cl^- profile. To sum it up: if our measurements are limited to only K^+ or Na^+ , the most reasonable assumption about the other ions are: The rise in K^+ is balanced with an equal decrease in Na^+

$$\Delta[\text{K}^+]^0 = -\Delta[\text{Na}^+]^0 \quad \wedge \quad \Delta[\text{Cl}^-]^0 = 0$$

Scenario 2: The rise in K^+ is shared between Na^+ and Cl^-

$$\Delta[\text{K}^+]^0 = -\frac{1}{2}\Delta[\text{Na}^+]^0 + \frac{1}{2}\Delta[\text{Cl}^-]^0$$

Scenario 3: The rise in K^+ is balanced with an equal increase in Cl^-

$$\Delta[\text{K}^+]^0 = \Delta[\text{Cl}^-]^0 \quad \wedge \quad \Delta[\text{Na}^+]^0 = 0$$

Scenario 4: In studies of spreading depression [7][8], It has been shown that the rise in Na^+ is even larger than the rise in K^+ , and that the charge is balanced by Cl^- . The ratios between the ion species makes the foundation for the fourth scenario:

$$2\Delta[\text{K}^+]^0 = -\Delta[\text{Na}^+]^0 \quad \wedge \quad \Delta[\text{K}^+]^0 = -\Delta[\text{Cl}^-]^0$$

Scenario 5: In some experiments, the concentrations of two different ion species are known. For this reason I have included a 5th scenario. Here, I assume that both $[\text{K}^+]$ and $[\text{Na}^+]$ are known, and make an assumption about Cl^-

$$\Delta[\text{K}^+]^0 + \Delta[\text{Na}^+]^0 = \Delta[\text{Cl}^-]^0$$

To evaluate which scenario describes the ionic concentration in the extracellular space best, I have used the following strategy. The data from the simulations of Halnes et al. [2] contains Na^+ , K^+ , Ca^{2+} and an unspecified anion X^- with the same properties as Cl^- . I have used this data set as a proxy for a real population of neurons. Then, I used the $[\text{K}^+]$ data from the same simulation to construct the initial ion concentration profiles for the four first scenarios, and simulated the diffusion potential for each of them. This made me able to compare each scenario to a "full model", and to see how

the assumptions of each scenario affected the diffusion potential. In Section 3.3 is a plot of the diffusion potentials of the constructed scenarios at $t = 0$ together with the diffusion potential resulting from the full model, and a discussion of each scenario.

Of the scenarios 1–4, scenario 1 gave the best fit with the full model. For this reason, I used the 1:1 Na^+/K^+ exchange assumption to construct initial concentration profiles based on the data of section 2.7, and simulated the diffusion potentials. The initial concentration profiles and the resulting potentials are presented in section 4.3.1.

3.4 The solution and its power spectrum density

A presentation of the diffusion potential is found in section 4.3.1, where I have used a contour plot of $\Phi(x, t)$ to illustrate the development of the potential with time. The potential, and the powers of the potential are not the same for all cortical depths. To find the power spectrum density of the diffusion potential, I used `periodogram` from the `signal` class in `scipy`. The input of `periodogram` is the sampling frequency $f_s = 1/\Delta t$ of the signal. It returns a vector of frequencies f , and the PSD of the signal. Both has length $f_s/2$.

I wanted to look at the largest possible effect of the diffusion potential on the total extracellular potential. For this purpose, I have defined the mean power of the signal at depth x_i as:

$$\overline{\text{PSD}_i} = \frac{2}{f_s} \sum_{k=0}^{f_s/2} \text{PSD}_{k,i} \quad (3.4)$$

The index of the maximum mean power is given by:

$$i_{\max} = \max_i \overline{\text{PSD}_i} \quad (3.5)$$

This was used to find the maximum mean power, $\text{PSD}_{\max} = \text{PSD}_{i_{\max}}$ and the depth where the maximum mean power was found, $d_{\max} = x_{i_{\max}}$.

PSD_{\max} of the diffusions potentials are presented in a log-log plot in section 4.3.2.

3.5 The quality of the solver

How good is the solver I have implemented? One important test is the electroneutrality test. I have implemented a unit test² to check that the sum

$$\frac{\sum_k z_k c_k}{\sum_k z_k^2 c_k}$$

does not exceed a certain value. I have set this value to 10^{-13} . Further testing is difficult, as there is no analytical solution to equation 2.8.

I have used the equivalence of the purely diffusive system and the electrodifflusive two-ion system described in section 2.10.1 to investigate the stability and the precision of the solver. I simulated the electrodifflusive system with the initial conditions

$$c_{Na}(x, 0) = c_{Cl}(x, 0) = 150 + 3 \cdot \sin(\pi x / L)$$

where concentrations are measured in mM and the diffusion coefficients are D_{Na} and D_{Cl} . This yielded the solutions for the concentrations

$$c_{\text{el.diff}} = c_{Na}(x, t) = c_{Cl}(x, t)$$

and a solution for the potential, $\Psi(x, t)$. Then, I simulated a system with two ion species which both have the same diffusion coefficient

$$D = 2D_{Na}D_{Cl}/(D_{Na} + D_{Cl})$$

but with opposite charge. The initial conditions were the same as in the just mentioned sodium-chloride system, the two equal solutions of this system are named c_{diff} .

With the initial conditions

$$c(x, 0) = 150 + 3 \cdot \sin(\pi x / L)$$

the solution of the purely diffusive system is given by Equation 2.21:

$$c(x, t)_{\text{analytical}} = 150 + 3 \sin \frac{\pi x}{L} \cdot e^{-D\pi^2 t / L^2}$$

²The code does not run if the criterion is not fulfilled

I found the difference between the analytical and the numerical solution for the purely diffusive system for various combinations of Δx and Δt , and I used the difference as an error estimate. The results are presented in section 4.1.

The two-ion system is a constructed system; it is not related to processes in the brain. I have used it to make sure that the solver works properly, by comparing the purely diffusive system to the two-ion system of.

Chapter 4

Results

4.1 Error analysis

I calculated the difference between the numerical solution of the electrodiffusive system, $c_{\text{el.diff}}(x, t)$, and the numerical solution of the purely diffusive system, $c_{\text{diff}}(x, t)$, for various combinations of Δt and Δx (the same combinations as in Table 4.1). I found the difference to be $\mathcal{O}(10^{-15})$. For the electrodiffusive system, there was also a diffusion potential, $\Phi(x, t)$, but for the purely diffusive system, the potential was zero at all depths for all times, and it is reasonable to call it a purely diffusive system. This is a confirmation of what was stated in section 2.10.1: the concentrations of the electrodiffusive two-ion system (the sodium-chloride system) behave exactly like the concentrations of the purely diffusive two-ion system, we call this solution $c_{\text{numerical}}$. In the following, I have performed an error analysis on $c_{\text{numerical}}$.

I have compared the analytical solution to the numerical solution. I tried with different values for the initial maximum concentration deviation, Δc_{max}^0 , and I found that the difference was proportional to the maximum concentration deviation. To study the error, I calculated the maximum value of

$$\frac{|c(x = 0.5, t)_{\text{numerical}} - c(x = 0.5, t)_{\text{analytical}}|}{\Delta c_{\text{max}}^0} \quad (4.1)$$

for various combinations of Δt and Δx , see Table 4.1. All simulations had $t_{\text{final}} = 100$ s and $L = 1$ mm. The error was $\mathcal{O}(\Delta x)^2$, which is in line with the error of the approximations I used for the spatial derivatives. The time derivative approximation had an error of $\mathcal{O}(\Delta t)$, but the solution did not seem to improve with smaller Δt . The stability criterion $\Delta t \leq (\Delta x)^2/2D$

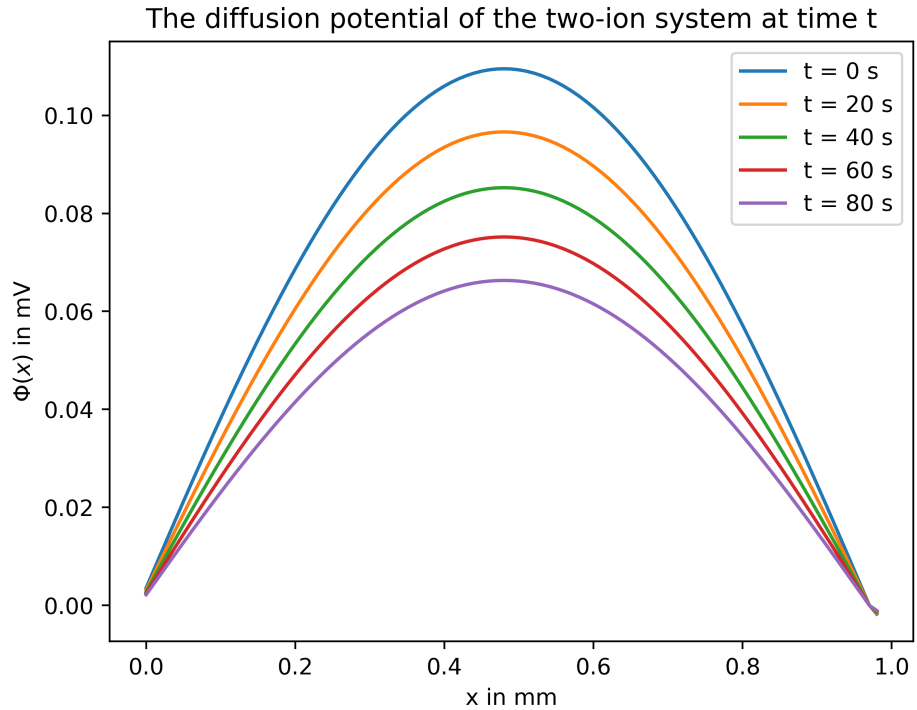


Figure 4.1: The simulated diffusion potential of a system with two ions, Cl^- and Na^+ with the initial concentrations: $c_{\text{Na}}(x, 0) = c_{\text{Cl}}(x, 0) = 0.15 + .003 \cdot \sin(\pi x/L)$. The diffusion potential has the same sine sine shape as the initial concentration, and the amplitude decays with time. $\Delta x = 0.01$ mm, $\Delta t = 0.01$ s.

with $D \sim 2 \cdot 10^{-9}$ and Δt and Δx in SI units gives the following constraint for Δt

$$\Delta x = 10^{-5} \rightarrow \Delta t \leq 10^{-1}/4$$

$$\Delta x = 10^{-6} \rightarrow \Delta t \leq 10^{-3}/4$$

which is illustrated Table 4.1. To meet the stability criterion for $\Delta x = 0.001$ mm, I need $\Delta t = 0.0001$ s. My implementation of the numerical scheme demands an array with dimensions $N_x \times N_t$. With my choices of t_{final} and L the array size is 100×1000000 . When I tried to do this, I ran out of memory, and was not able to calculate the error. The combination of $\Delta x = 0.001$ mm and $\Delta t = 0.0001$ s is therefore represented by a question mark in Table 4.1. Since there is nothing to gain with a high time resolution, I have used $\Delta t = 0.01$ s and $\Delta x = 0.001$ mm for all simulations presented in the following.

This gives an error of $\mathcal{O}(10^{-5})$.

Table 4.1: The difference between the numerical and the analytical solution relative to the initial concentration deviation. $\Delta x = 0.1$ mm yields an error of $\mathcal{O}(10^{-3})$, $\Delta x = 0.01$ mm yields an error of $\mathcal{O}(10^{-5})$, but is unstable for $\Delta t = 0.1$ s. All simulations have $L = 1$ mm, $t_{\text{final}} = 100$ s, $\Delta c_{\max}^0 = 3$ mM.

$\Delta t/\Delta x$	0.1 mm	0.01 mm	0.001 mm
0.1 s	0.003426	unstable	unstable
0.01 s	0.003546	1.757e-05	unstable
0.001 s	0.003558	2.713e-05	unstable
0.0001 s	0.003559	2.808e-05	?

So far, we have only looked at the solution for the concentrations, and seen that

$$c(x, t) = c^0 + \Delta c_{\max}^0 \sin \frac{\pi x}{L} \cdot e^{-D\pi^2 t/L^2}$$

is a solution of the sodium-chloride system. What about the solution for the potential, $\Phi(x, t)$? In Figure 4.1 I have plotted $\Phi(x, t)$ for $t = 0, 20, 40, 60, 80$ s. $\Phi(x, t)$ retained a sine shape for all t . I found the amplitude at $t = 0$ to be $\Phi_{\max} = 0.1095$ mV. With $\tau = L^2/D\pi^2 = 158.2$ s, I calculated

$$\Phi_{\max} \cdot e^{-t/\tau}$$

and compared it to the solution $\Phi(L/2, t)$, see Table 4.2. An exponentially decaying concentration gave an exponentially decaying potential¹. This insight comes in handy in section 4.4, but we must keep in mind that the exponential concentration decay is a property of the very simplified sodium-chloride system, where the initial concentration had only one maximum and the shape of a sine function.

Table 4.2: The numerical solution $\Phi(x, t)$ at the midpoint of the system and an exponentially decaying function with $\tau = 158.2$ s for $t = 0, 20, 40, 60, 80$ s. The numerical solution was decaying exponentially.

	$t=20$ s	$t=40$ s	$t=60$ s	$t=80$ s
$\Phi(L/2, t)$	0.0966 mV	0.0852 mV	0.0751 mV	0.0663 mV
$\Phi_{\max} \cdot e^{-t/\tau}$	0.0965 mV	0.0851 mV	0.0750 mV	0.0661 mV

¹The value of $\Phi_{\max} \cdot e^{-t/\tau}$ differs slightly from $\Phi(L/2, t)$. This is caused by the parameter L , which theoretically is 1 mm, but in the numerical solution it is $(N_x - 1)\Delta x = 0.99$ mm

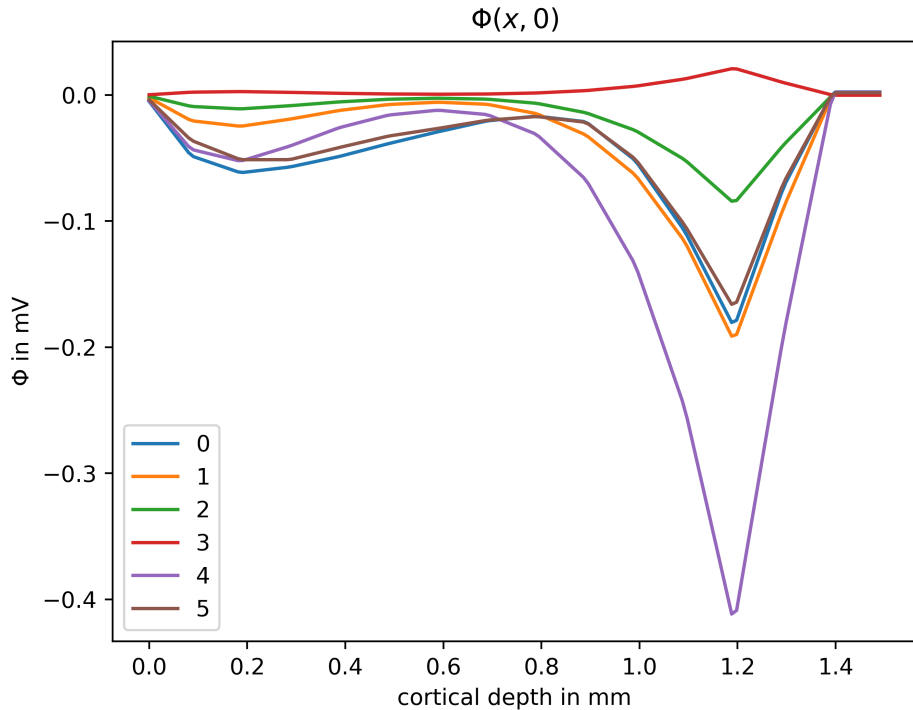


Figure 4.2: The diffusion potential at $t = 0$ s for the full model (legend 0), and scenario 1 – 5. Scenario 5 (where both $[K^+]$ and $[Na^+]$ is known) has the best fit. Of the scenarios based on only known $[K^+]$, scenario 1 is the best. The spreading depression scenario (scenario 4) gives a much larger potential than the full model in the soma region (depth $x = 1.2$ mm).

4.2 Evaluation of the scenarios for the initial concentration profiles

The error analysis of the previous section gave me confidence that my numerical scheme does indeed simulate the diffusion potential. The next challenge was to find initial conditions in agreement with biological systems. As discussed in section 3.3, the recordings of the laminar concentrations profiles does not contain information about more than two ion species, and for my simulations to be realistic I need at least three. I have tested the 5 initial ion concentration scenarios of section 3.3.

4.2.1 The shape of the diffusion potential at $t = 0$

The blue line (with legend 0) in figure 4.2 is the diffusion potential at $t = 0$ s calculated from the full model with data from the Halnes et al. [2]. The other lines are the diffusion potentials at $t = 0$ s for the five scenarios, where $[K^+]^0$, and in scenario 5, $[Na^+]^0$, were taken from the same data set.

For all scenarios, the potential was largest at a cortical depth of approximately 1.2 mm. This correspond to the soma compartment of the neurons in simulations. The soma compartment has the largest ionic exchange with the extracellular space, hence the large diffusion potential. For cortical depths between 0.8 and 1.3 mm, scenario 1 also seemed to give a good agreement with the full model. In this region, the ionic exchange consist mainly of K^+ and Na^+ . In the higher regions, the difference was larger, because the K^+ efflux from the neurons in this region is small, compared to the Na^+ influx to the neurons.

The potential of scenario 2 had the same shape as that of scenario 1, but a smaller amplitude. The smaller amplitude can be explained by the diffusion coefficients. The diffusion coefficients D_K and D_{Cl} are much closer to each other than D_K and D_{Na} (The values of the diffusion coefficients can be found in Table 3.1). The difference in diffusion coefficients is what makes the diffusion potential in the first place. When half of the Na^+ is replaced with Cl^- , half of the K^+ is practically neutralized by Cl^- , effectively halving the initial concentration deviation. The result is that scenario 2 had poorer fit than scenario 1, for all cortical depths.

In scenario 3, we see the consequences of the very small difference between D_{Cl} and D_K . Here, the diffusion potential was 12% of the full model potential. A peculiarity of this scenario is that the potential was positive. The explanation can be found in the diffusion coefficients. D_{Cl} is larger than D_K , so that the negative Cl^- escapes faster, leaving a positive charge in the soma region. In the scenario where $[Na^+]^0$ is largest, the diffusion potential is largest. In the scenario where $[Na^+]^0 = 0$, K^+ and Cl^- diffuse with almost the same speed, and the potential required for maintaining electroneutrality is much lower.

The spreading depression scenario (scenario 4) stands out. The amplitude of the diffusion potential in the soma region was more than twice the amplitude from the full model. This is caused by $\Delta[Na^+]^0$, which is the double of $\Delta[K^+]^0$. There was a good fit between the spreading depression scenario

and the full model in the higher regions. By revisiting the laminar profile of all the ion species in figure 2.4, upper right subpanel, we see that the ionic exchange is in fact of the same ratios as in the spreading depression scenario. At cortical depths where $\Delta[\text{Cl}^-]^0$ is approximately zero or slightly positive, the spreading depression scenario overestimates the diffusion potential drastically, but at depths where $\Delta[\text{Cl}^-]^0 < 0$, the spreading depression scenario gives a better fit than the 1:1 Na^+/K^+ exchange (scenario 1).

Of the four scenarios based only on a known $[\text{K}^+]$, scenario 1 had the best fit in the soma region, where the potential was at its largest. In the upper cortical regions, scenario 4 had a better fit, but because it was far off in the soma region, I believe that scenario 1 (the 1:1 Na^+/K^+ exchange) is the most suitable scenario for populations of neurons with ionic output similar to that of the simulations by Halnes et al..

Scenario 5 is not a realistic scenario, in that none of the data sets contain laminar profiles of both Na^+ and K^+ . Nevertheless, the good fit between scenario 5 and the full model indicates that it is sufficient to know the concentrations of these two ion species to get a satisfying model of the diffusion potential. In scenario 5, $\Delta[\text{Cl}^-]^0$ was found by $\Delta[\text{K}^+]^0 - \Delta[\text{Na}^+]^0 = \Delta[\text{Cl}^-]^0$, but in the full model the relation was $\Delta[\text{K}^+]^0 - \Delta[\text{Na}^+]^0 - 2[\text{Ca}^{2+}]^0 = \Delta[\text{Cl}^-]^0$. In other words, the difference between the two is Ca^{2+} . I think the good fit between scenario 5 and the full model justifies the assumption that Ca^{2+} is negligible.

4.2.2 The PSD of the diffusion potential

The main concern of this thesis is not the spatial shape of the diffusion potential, but its time varying aspects, represented by its PSD. I found the maximum mean power, PSD_{\max} (defined in Section 3.4), of each scenario, and plotted it as a log-log plot, see left panel of figure 4.3. The depth d_{\max} was 1.18 mm for all scenarios, which corresponds to the soma compartment. At this depth, the difference between the full model and scenario 1 was small.

Based on the potentials in figure 4.2, we should expect the largest difference between the full model and scenario 1 to be at a depth of 0.2 mm. In the right panels of figure 4.3 I have included the PSDs at this depth. At the depth of 0.2 mm, the powers of the scenario 1 potential were smaller than the powers of the full model. However, the PSD at 0.2 mm of the full model potential was almost ten times smaller than PSD_{\max} of the full model

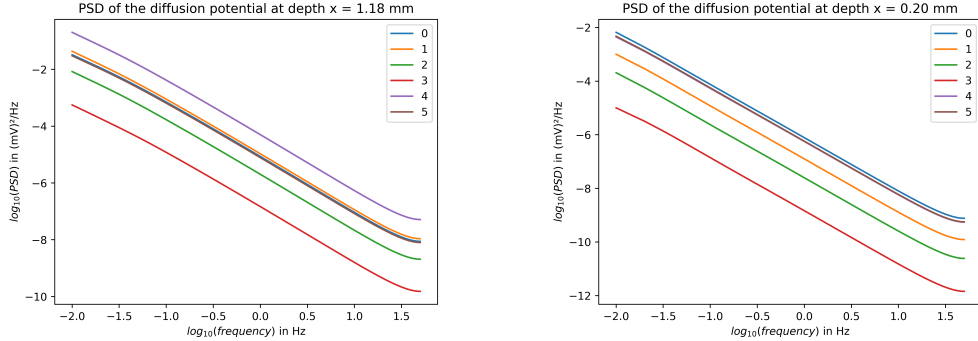


Figure 4.3: Left: The PSDs of the diffusion potentials at cortical depth $x = 1.18$ mm. The spreading depression scenario (5) has larger powers than the scenarios. Scenario 1 and scenario 5 gives a diffusion potential with the same powers as the full model (0). Right: The PSDs of the diffusion potentials at cortical depth $x = 0.2$ mm have smaller powers than at $x = 1.18$ mm for all scenarios. The diffusion potential of scenario 1 have smaller powers than the full model. The scenario 4 and 5 gives the same PSD (the purple line is hidden under the brown line).

potential. I think that scenario 1 gives a good estimate when looking for the maximum possible effect of the diffusion potential on the local field potential.

4.3 The diffusion potentials calculated from K^+ profiles from four different experiments

4.3.1 The shape of the initial concentration profile and of the diffusion potential

Of the four scenarios for the initial concentration profiles based on a known K^+ concentration, I think scenario 1 is the best, and I have used the 1:1 Na^+/K^+ exchange to infer the initial concentration profiles of the unknown ion species. Figure 4.4 shows the initial concentration profiles, together with the data points I have used to construct the profiles. The data points are taken from figure 2.4, and are marked as black dots. Figure 4.5 shows contour plots of the resulting diffusion potentials. I have labeled the concentration profiles and the potentials after the publication where the data is taken from.

The cortical depth where the largest potential was found, d_{\max} , seemed to correspond with the depth at which initial maximum deviation from baseline K^+ , $\Delta[\text{K}^+]^0$, was largest. Because I have used the scenario where $\Delta[\text{K}^+]^0$

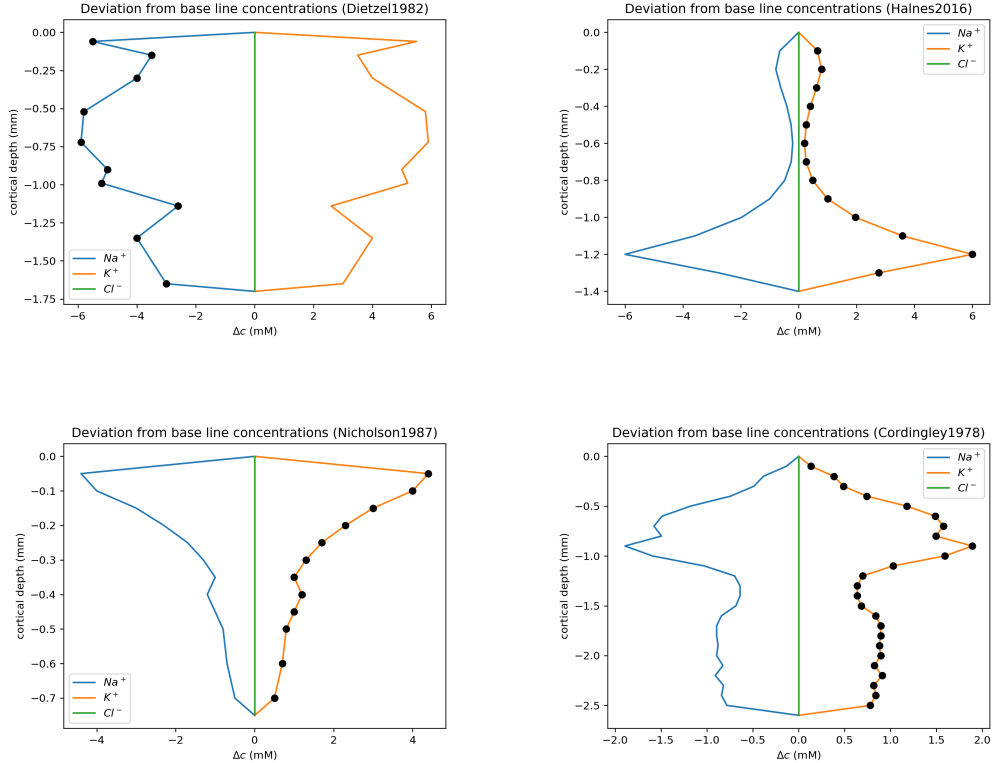


Figure 4.4: Initial ion concentration profiles. Black dots represent the original data points. Upper left: Na^+ profile recorded from sensimotori cortex of cats by Dietzel et al. Lower left: $[\text{K}^+]$ recorded from cerebellar cortex of cats by Nicholson et al. Upper right: K^+ simulated by Hahn et al., using 10 pyramidal neurons. Lower right: K^+ recorded from visual cortex of cats by Cordingley and Somejen, data is modified by Gratiy et al.

mirrors $\Delta[\text{Na}^+]^0$, and $\Delta[\text{Cl}^-]^0 = 0$, the initial maximum deviation from baseline will be at the same depth for all ion species k , hereafter referred to as Δc_{\max}^0 . By comparing Figure 4.4 and Figure 4.5, I found that the simulation with the largest Δc_{\max}^0 , also gave the largest $\Psi(x, 0)$. To give further support to this idea, I returned to Equation 2.10. By assuming that the conductivity $\sigma = \frac{F}{\lambda_n^2 \Psi} \sum_k z_k^2 D_k c_k$ is roughly constant [2], we have the approximation

$$\frac{\partial \Phi}{\partial x} \propto \sum_k z_k D_k \frac{\partial c_k}{\partial x} \quad (4.2)$$

which leads to a relation between $\Delta\Phi$ and Δc_k :

$$\Delta\Phi \propto \sum z_k D_k \Delta c_k \quad (4.3)$$

where $\Delta\Phi$ is the difference between potential at the boundary and some point inside the system, and Δc_k is the deviation from baseline concentration for ion species k .

Relation 4.3 can by no means be used to calculate Φ , as the simplification $\sum_k z_k^2 D_k c_k = \text{constant}$ is not true, and should only be regarded as a justification of the intuitive idea that the simulations with the largest Δc_{\max}^0 produces the largest potentials.

Also, a sharp peak in the initial concentration gave a sharp peak in the potential at $t = 0$ (like the the potentials with initial concentrations from Nicholson et al. and Haldnes et al.), while a smoother initial concentration profile (like the profiles based on concentrations from Dietzel et al. and Coringley & Somjen) gave a smoother potential. The potentials decayed with time, but the way they decayed depended on the shape of the initial concentration profile. In the simulations with a relatively smooth initial concentration, after the first 10 s or so, the potential seemed to be decaying monotonously, indicating that an exponential decay might be a reasonable model for the diffusion potential. In the case of a sharp peak in the initial concentration, the potential was also "spreading out", e.g. at some points the potential was temporarily increasing. This means that assuming an exponential decay of the potential will not be correct if there is a sharp peak in the initial concentration. Still, at the location of the concentration peak, the concentration was monotonously decaying, and for this location the potential might be described in terms of an exponential decay towards zero.

4.3.2 The PSD of the diffusion potential

For each of the four simulations, I found PSD_{\max} and the corresponding depths, d_{\max} . I calculated $\log \text{PSD}_{\max}$ at 1 Hz, the results are listed in Table 4.3, together with d_{\max} and Δc_{\max}^0 . From Table 4.3 we can see that the larger Δc_{\max}^0 , the larger were the powers of the signal. By comparing d_{\max} to the concentration profiles in Figure 4.4 we can see that d_{\max} was the same as the depth of Δc_{\max}^0 .

Figure 4.6 shows a log-log plot of the PSD_{\max} of the four diffusion poten-

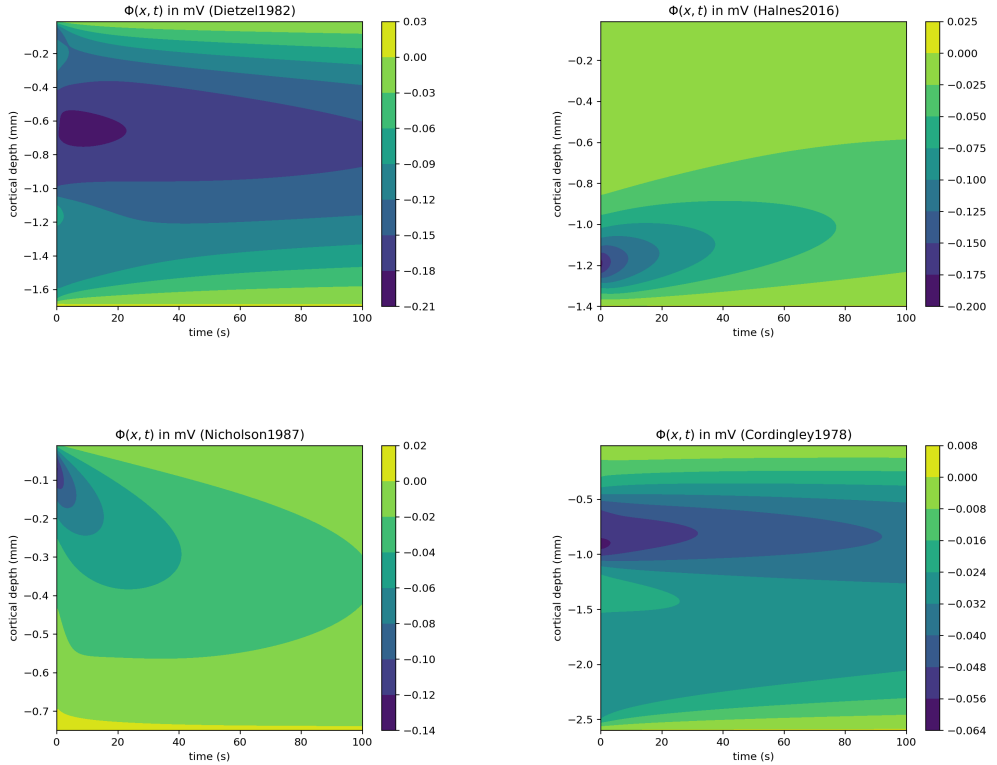


Figure 4.5: The diffusion potentials calculated from the initial concentration profiles. The shape of the initial concentration profile is reflected in the shape of the diffusion potential. NB: note that the colorbar is unique for each plot.

Table 4.3: The power of the diffusion potentials at 1 Hz. The power is higher when the largest initial deviation from baseline concentration, Δc_{\max}^0 , is higher, and the largest powers are found at the depth where the magnitude of the diffusion potential is large.

Data set	$\log(\text{PSD}_{\max})$	Δc_{\max}^0	d_{\max}
Halnes et al.	-4.89	6.0	1.18 mm
Dietzel et al.	-5.21	5.9	0.08 mm
Nicholson et al.	-5.32	4.4	0.10 mm
Cordingley & Somjen	-6.63	1.89	0.88 mm

tials presented in the previous section. For frequencies larger than 0.1 Hz, the lines of figure 4.6 appear parallel. I used linear regression, and found that this was the case for frequencies between 0.1 and 10 Hz. The slope of all four PSDs was -2.00, with three leading digits and a mean squared error of $\mathcal{O}(10^{-5})$. A slope of -2 in the log-log space translates to a $1/f^2$ frequency

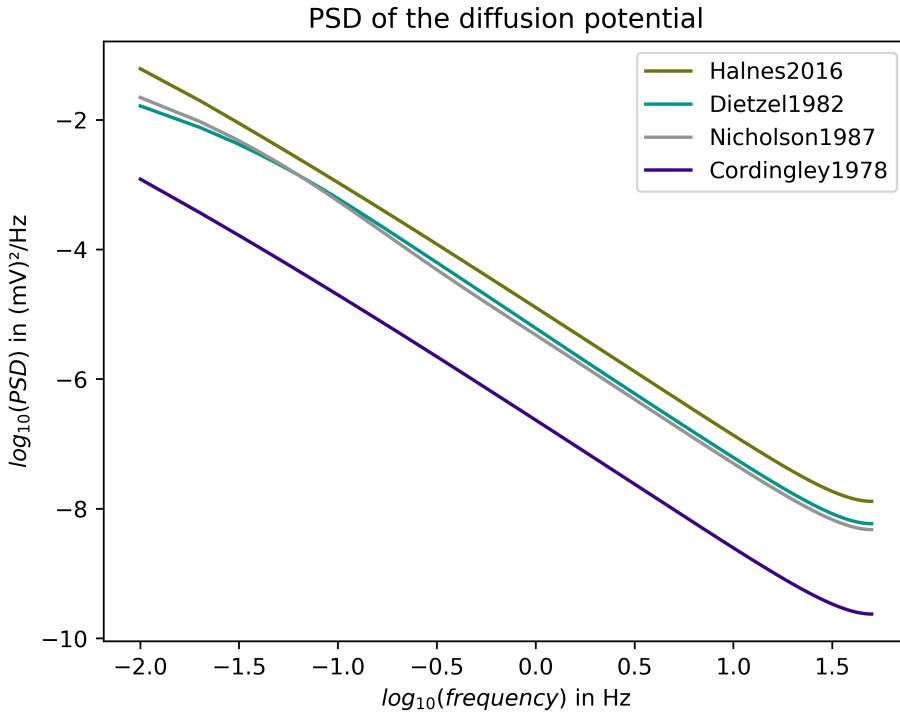


Figure 4.6: The PSD of the diffusion potentials. For frequencies between 0.1 and 100 Hz, all PSDs follow a $1/f^2$ power law. The largest initial concentration deviation in the data from Hahn et al., and this produces the largest powers.

dependence. This is commonly referred to as a $1/f^2$ power law. It has been proposed that the diffusion potential follows a $1/f^2$ power law [2]. My results supports this proposal for frequencies between 0.1 and 10 Hz. The shape of the initial concentration profile did not affect this power law. This may be because my algorithm looked for the depth where the mean power was largest, and that at this location the potential was monotonously decaying.

4.3.3 The PSD of the diffusion potential compared to PSDs of local field potentials

Previous studies suggested that diffusion could affect the low frequency components (smaller than 1 Hz) of the LFP in scenarios with large, but not pathologically large, concentration gradients [2][3]. In figure 4.7, I have plotted the PSDs of figure 4.6 together with the PSD of the local field potential

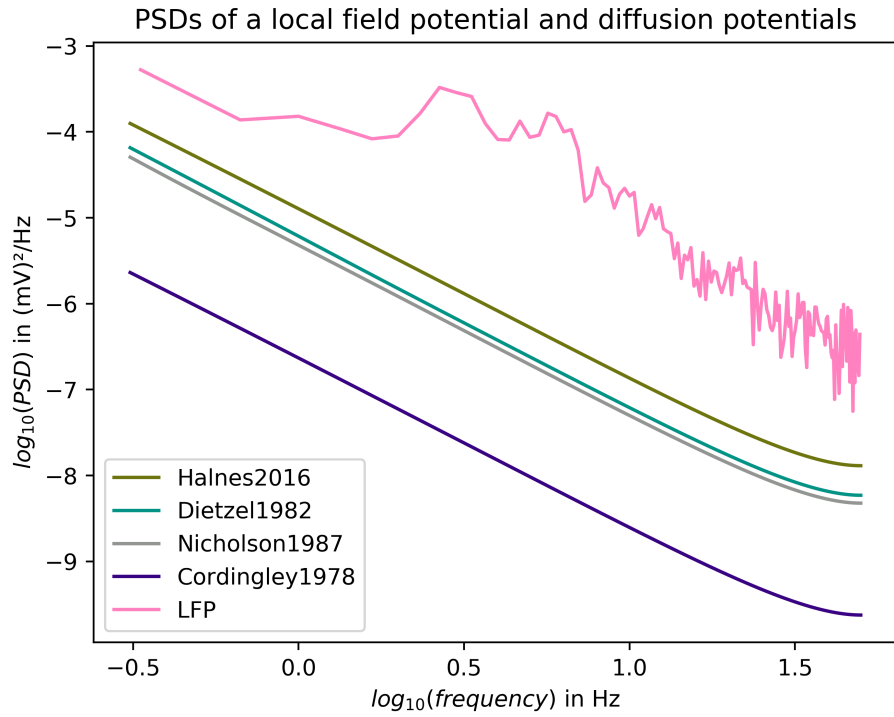


Figure 4.7: The local field potential from visual cortex in mice (pink line). PSDs of diffusion potentials resulting from recorded ion concentration profiles, the same PSDs as in figure 10. The powers of the diffusion potentials are smaller than the powers of the LFP.

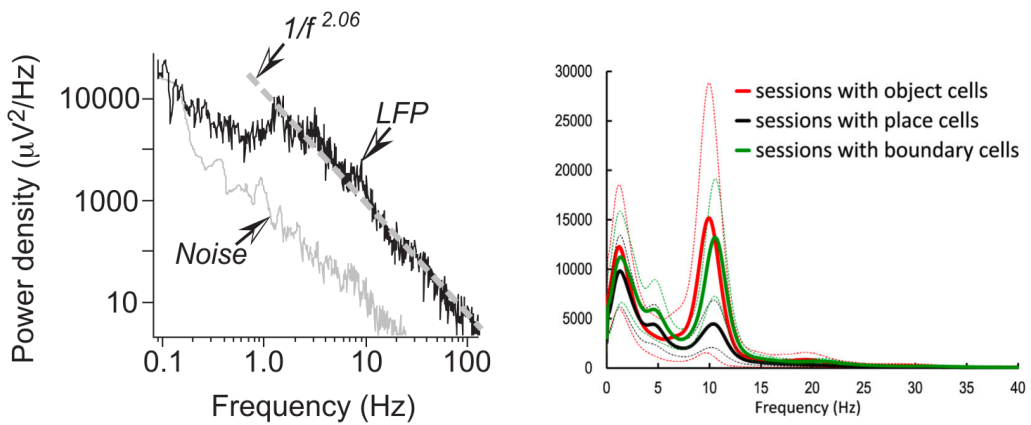


Figure 4.8: Left: PSD of a LFP recorded in somatosensory cortex of rats [21] Right: PSD of a LFP from anterior claustrum of rats [22]. Axis labels applies to both figures.

adapted from Gratiy et al. [3]. The recordings are from the primary visual cortex of mice when exposed to a light source which is turned off and on. I have omitted the lowest frequencies of the diffusion potentials and the highest frequencies of the LFP to make it so that the PSDs are plotted for the same frequency range. From figure 4.7 it is clear that the diffusion potentials have lower powers than the LFP - for all frequencies. The diffusion potential is too small to compete with all the other slow potentials in the extracellular space. In figure 4.8 are two other examples of PSDs of LFPs. At 1 Hz, the power is above 10^{-3} mV²/Hz for both LFPs, with is a much larger value than the powers of the diffusion potentials (see Table 4.3).

4.4 Exponential $\Delta[\text{K}^+]$ decay

So far, I have explained the ion transport in the extracellular space solely by the joint effort of electrical migration and diffusion. This is not the case in living systems. Many mechanisms contribute to the maintenance of low concentration gradients, such as ionic pumps, ion exchangers and co-transporters [5], and uptake and buffering performed by astrocytes [20]. We can therefore expect the gradients to have a more rapid decay. It would be a time-consuming task to model all these processes. To test the effect of faster concentration dynamics on the diffusion potential, I have instead made a model which allows the concentration gradients to decay exponentially, where the time constant τ is a model parameter. The model is based on a 1:1 Na⁺/K⁺ exchange, and the concentration dynamics are:

$$c_K(x, t) = c_K^0 + \Delta c_{\max}^0(x) \cdot e^{-t/\tau}$$

$$c_{Na}(x, t) = c_{Na}^0 - \Delta c_{\max}^0(x) \cdot e^{-t/\tau}$$

$$c_{Cl}(x, t) = c_{Cl}^0$$

where c_K^0 , c_{Na}^0 and c_{Cl}^0 are the baseline concentrations, and $\Delta c_{\max}^0(x) = \Delta[\text{K}^+]^0 = -\Delta[\text{Na}^+]^0$. Then, I have used the discretized version of

$$\frac{\partial}{\partial x} \Phi = \frac{-\Psi \sum_k z_k D_k \frac{\partial}{\partial x} c_k}{\sum_k z_k^2 D_k c_k}$$

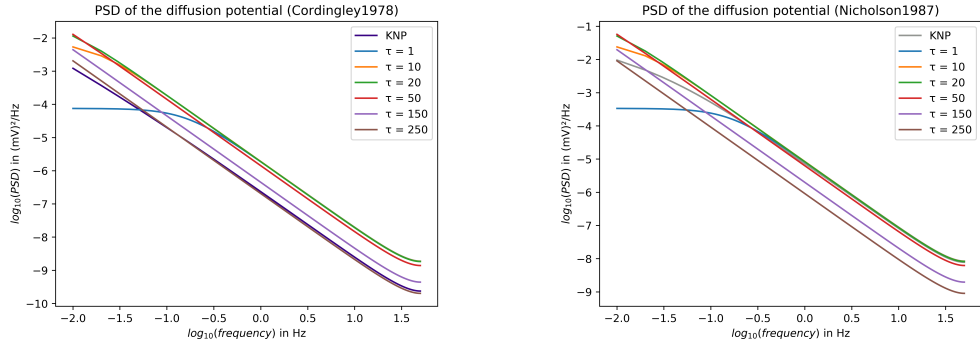


Figure 4.9: PSDs of the KNP diffusion potential (legend KNP) and of the ED diffusion potential (the legend is the time constant of the ΔK^+ and ΔNa^+ decay). Decreasing the time constant increases the powers. All PSDs exhibit the $1/f^2$ power law for most frequencies, but time constants ~ 10 s or smaller, gives a PSD that does not follow the $1/f^2$ power law for the lowest frequencies. Left: Initial concentrations from Cordingley & Somjen. The KNP diffusion potential has approximately the same PSD as the ED diffusion potential with $\tau = 250$ s. Right: Initial concentrations from Nicholson et al.. The KNP diffusion potential has approximately the same PSD as the ED diffusion potential with τ between 1 s and 10 s.

(equation 3.1) to calculate the momentary diffusion potential at every time step. I simulated this exponential decay (ED)² diffusion potential with initial concentrations from 1) Cordingley & Somjen [4], and 2) Nicholson et al. [11]. I have used time constants $\tau = 1, 10, 20, 50, 150, 250$ s. I calculated PSD_{max} in the same fashion as described in section 3.4. The results are shown in figure 4.9, together with the PSD_{max} of the KNP diffusion potentials simulated with the same initial concentrations.

The ED diffusion potentials followed approximately the same $1/f^2$ power law as we have seen in previous sections. This indicates that the modelling of the diffusive process itself might not be necessary, as exponentially decaying concentration gradients exhibited the same properties when it comes to the PSD of the potential. The important part is to find the correct τ . With the initial concentrations from Cordingley & Somjen, the PSD of KNP diffusion potential seemed to fit well with the PSD of the ED diffusion potential that had $\tau = 250$ s. This is larger than the theoretical time constant of the

²I will use the abbreviation ED to separate the diffusion potential caused by exponentially decaying concentration deviations from the diffusion potential found with the KNP formalism.

sodium-chloride system (which had $\tau = 158.2$ s), but of the same order of magnitude. With the initial conditions from Nicholson et al., the best fit was for τ somewhere between 1 and 10 s. I believe the reason is the steep concentration gradient. We saw that the potential was spreading out, which indicates that the concentrations also are spreading out, and that the concentration deviation is decaying faster in the peak location because of this. However, most of this effect is probably an artefact of the boundary conditions, which imposes a rapid decay at points close to the boundary.

How does the choice of τ affect the PSD of ED diffusion potential? Figure 4.9 suggest that τ affect the powers of the diffusion potential. The smaller the time constant, the higher powers, but only up to a limit. It seems like $\tau \sim 20$ s, gives the largest powers. With an even smaller τ , the slope of the PSD is approaching zero for the lowest frequencies. This is not shocking news: a fast-varying signal should yield lower powers for the lowest frequencies. What is less intuitive, is that the powers does not appear to be higher for any frequency. To get an better understanding of this, I have found a relation between the logarithm of the PSD, the frequency, and the time constant of an exponential function defined by:

$$v(x) = \begin{cases} 0 & \text{for } t < 0 \\ v(t) = e^{-t/\tau} & \text{for } t \geq 0 \end{cases} \quad (4.4)$$

The fourier transform of $v(t)$ is

$$\mathcal{F}(v(t)) = \frac{1}{\frac{1}{\tau} + i2\pi f}$$

The absolute value of $\mathcal{F}(v(t))$:

$$|\mathcal{F}(v(t))| = \frac{1}{|\frac{1}{\tau} + i2\pi f|} = \frac{1}{\sqrt{\frac{1}{\tau^2} + (2\pi f)^2}}$$

Squaring $|\mathcal{F}(v(t))|$:

$$|\mathcal{F}(v(t))|^2 = \frac{1}{\frac{1}{\tau^2} + (2\pi f)^2}$$

The PSDs are often presented as log-log-plots.

$$\log |\mathcal{F}(v(t))|^2 = \log \frac{1}{\frac{1}{\tau^2} + (2\pi f)^2} = -\log(\frac{1}{\tau^2} + (2\pi f)^2)$$

If τ is large the slope of $\log \text{PSD}(\log f)$ is approximately -2

$$\log |\mathcal{F}(v(t))|^2 \approx -2 \log(2\pi f)$$

If τ is small, $1/\tau^2$ will dominate when the frequencies are small

$$\log |\mathcal{F}(v(t))|^2 \approx -\log(\frac{1}{\tau^2}) = \text{constant}$$

which confirms the above stated relations.

We have seen that the ED diffusion potential could have higher powers than the KNP diffusion potential. The half-lives of $\Delta[\text{K}^+]$ observed in experiments (see Section 2.7.3) yield $\tau \sim 0.7 - 7$ s. This means that the orange lines in Figure 4.9 might be closer the realistic diffusion potential, and that the realistic diffusion potentials have higher powers than what we saw in Section 4.3.2. At 1 Hz, the power of the recorded LFPs [3][21][22] was above 10^{-4} , which is much larger than the power of any of the PSD_{\max} of the ED diffusion potentials. Even with an arbitrary fast decay towards baseline, the powers of the diffusion potential were smaller than the powers of the recorded LFPs.

4.5 Spreading depression

As we saw in section 4.3, the magnitude of the diffusion potential, and thereby its power, is determined by the Δc_{\max}^0 . Concentrations measured in normal neuronal activity were not high enough to get powers as large as those we see in measurements of local field potentials. But in some extreme situations, like spreading depression, the concentration deviation gets much larger. I have simulated the diffusion potential with the initial K^+ profile recorded during spreading depression [8]. For Na^+ and Cl^- I used $\Delta[\text{Na}^+]^0 = -2\Delta[\text{K}^+]^0$ and $\Delta[\text{Cl}^-]^0 = -\Delta[\text{K}^+]^0$. The baseline concentrations were respectively 3 mM, 150 mM and 153 mM. This gave a maximum diffusion potential of -4.2 mV. This is similar to what was estimated with the help of the Goldman equation (Equation 2.1) [8]. Because the excessive K^+ is cleared out in

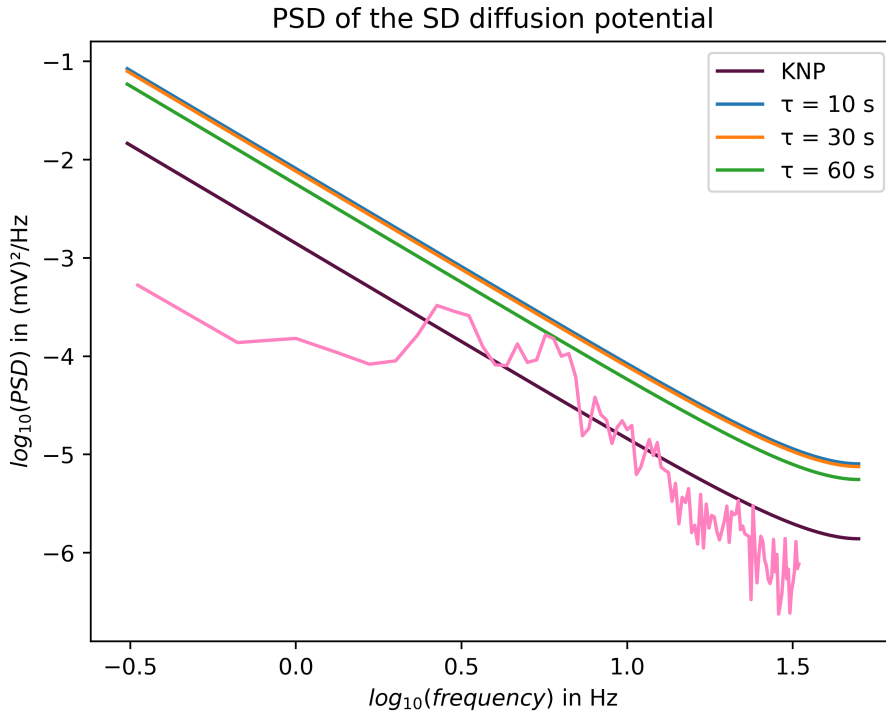


Figure 4.10: The local field potential from visual cortex in mice (pink and lavender line) together with PSD_{\max} from spreading depression concentration gradient. Plum line: diffusion potential simulated with KNP scheme, green, orange and red line: diffusion potential simulated with exponentially decaying $\Delta[\text{Na}^+]$, $\Delta[\text{K}^+]$ and $\Delta[\text{Cl}^-]$.

about a minute [7], I also simulated the diffusion potential from exponentially decaying concentrations, with time constants $\tau = 10, 30, 60$ s. The PSD_{\max} of these potentials, together with the PSD_{\max} from the KNP diffusion potential, are presented in Figure 4.10. I have included the same LFPs as in Figure 4.7 for comparison. Now, the diffusion potential is of the same, or even higher powers than the measured LFP for almost all frequencies in the range $\sim 0.3 - 30$ Hz, and diffusion might contribute to the total potential. I have not seen any LFPs recorded during spreading depression. It is possible that these LFPs have larger powers for the low frequencies than what is observed during normal activity.

Chapter 5

Discussion

5.1 Properties of the diffusion potential

Neuronal activity may cause local changes in the extracellular ionic concentrations. Diffusion along the concentration gradients may give rise to what we call the diffusion potentials. In this work I have simulated the extracellular diffusion potentials that would be associated with the extracellular concentration gradients seen in four different experiments. These simulations showed that the magnitude of the diffusion potential is related to the maximum deviation from baseline concentrations, and that the largest diffusion potential is found at the cortical depth where the concentration deviation is largest.

At this depth, the diffusive process was well approximated by an exponential decay of the extracellular concentration gradient, given a suitable choice for the time constant τ . For a steep concentration gradient, the time constant was up to 100 times smaller than for a flatter initial concentration profile. The restoring of baseline concentrations is often much faster than what diffusion accounts for.

The similarity between the PSD of the KNP-diffusion potential and the exponential decay (ED) diffusion potential have made me think that future modelling of the diffusion potential caused by extracellular concentration gradients can be approximated by exponentially decaying concentration gradients instead of the KNP formalism. The benefit of this approach is three-fold. Firstly, it allows for realistic time constants. A model that successfully predicts the effect of diffusion on the LFP, needs realistic time constants, because the choice of the time constant had an impact on both the powers of

the signal and the power law. Secondly, the model with exponentially decaying concentration gradients does not require a spatial dimension. In models used to simulate large networks of neurons interacting with the extracellular space and perhaps other cell types, the neuron may be modelled as one compartment without a spatial dimension. With the exponential decay, it is possible to include diffusion and the diffusion potential in such a model. Thirdly, it is easier to implement, faster to compute, and there is no stability criterion.

The log-log plots of the PSD of the diffusion potential at the depth where the potential was largest, had a slope of approximately -2 , which is the slope of the PSD of an exponentially decaying function, for frequencies above a certain limit, where this limit is determined by the time constant. This supports the modelling of the diffusion potential, not only the concentrations, as an exponentially decaying function. An estimate of the time constant will give an indication of in which frequency range the diffusion potential, or any other exponentially decaying potential, follows a $1/f^2$ power law, and in which range it is "flat". Previous studies have identified a $1/f^2$ power law for the LFP (frequencies up to 100 Hz), and explained this scaling as the result of a step-function of periods with 'bursting' neurons and 'pausing' neurons [21]. In those studies, the recording sessions lasted from 5-20 minutes. It is possible that concentration gradients were built up during the experiment, and that diffusion might have something to do with the $1/f^2$ scaling. This of course only speculation, and it implies that the concentration gradients must have been much higher than the recorded concentration gradients I have studied.

5.2 The effect of the diffusion potential on the local field potential

For the comparison of the PSD of the LFP and the diffusion potentials, I used recorded LFPs [3][21][22] and recorded extracellular concentration profiles [10][11][4] together with data from simulations of a small population of neurons [2]. I saw that the diffusion potentials had lower powers than the LFP for the range of frequencies included in the recordings. Based on these observations, I cannot say that the diffusion potential is likely to influence the LFP in the recordable frequency range. It might be so that the diffusion

potential contributes more to the LFP for below 0.3 Hz. This depends on the time constant, but also on other possible signals in the extracellular space with high powers in this frequency range.

A natural way to improve this study would be to include a larger set of recorded PSDs in the analysis. There is a lot of PSDs of LFPs available in the literature, but in most cases they are presented with arbitrary units, or a normalized signal, which makes them inadequate for a direct comparison with the PSD of the simulated diffusion potential. There might be regions in the brain where the neuronal activity contributes less to the LFP. This could be a region where the neural population density is lower, or a region where the synaptic input to the neurons is less frequent. Recordings from such a region could lead to other conclusions regarding the relative contribution from diffusive effects.

The same is true for recordings of the LFP in a situation where we can expect large gradients. Spreading depression is the extreme example of a situation with large gradients. In my simulations, the diffusion LFP of spreading depression was larger than recorded LFP. It would be very interesting to explore the LFPs recorded during spreading depression. If a $1/f^2$ power law is found for the lowest powers, it might indicate that spreading depression is a scenario where extracellular potentials to a large degree reflect diffusion.

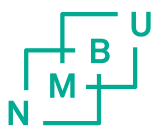
Chapter 6

Bibliography

- [1] Halnes, G., Østby, I., Pettersen, K.H., Omholt, S.W. and Einevoll, G.T., 2013. Electrodiffusive model for astrocytic and neuronal ion concentration dynamics. *PLoS computational biology*, 9(12), p.e1003386.
- [2] Halnes, G., Mäki-Marttunen, T., Keller, D., Pettersen, K.H., Andreassen, O.A. and Einevoll, G.T. (2016) 'Effect of ionic diffusion on extracellular potentials in neural tissue', *PLoS computational biology*, 12(11), p.e1005193.
- [3] Gratiy, S.L., Halnes, G., Denman, D., Hawrylycz, M.J., Koch, C., Einevoll, G.T. and Anastassiou, C.A. (2017) 'From Maxwell's equations to the theory of current-source density analysis', *European Journal of Neuroscience*, 45(8), pp.1013-1023.
- [4] Coldingley, G.E. and Somjen, G.G. (1978) 'The clearing of excess potassium from extracellular space in spinal cord and cerebral cortex', *Brain research*, 151(2), pp.291-306.
- [5] Purves, D. et al. (2012) *Neuroscience*. 5th edn. Sunderland: Sinauer Associates
- [6] Einevoll, G.T., Kayser, C., Logothetis, N.K. and Panzeri, S. (2013) 'Modelling and analysis of local field potentials for studying the function of cortical circuits', *Nature Reviews Neuroscience*, 14(11), p.770.
- [7] Ayata, C. and Lauritzen, M. (2015) 'Spreading depression, spreading depolarizations, and the cerebral vasculature', *Physiological reviews*, 95(3), pp.953-993.

- [8] Herreras, O. and Somjen, G.G. (1993) 'Analysis of potential shifts associated with recurrent spreading depression and prolonged unstable spreading depression induced by microdialysis of elevated K⁺ in hippocampus of anesthetized rats', *Brain research*, 610(2), pp.283-294.
- [9] 'Soma (biology)'(2015) *New World Encyclopedia*. Available at: [http://www.newworldencyclopedia.org/entry/Soma_\(biology\)](http://www.newworldencyclopedia.org/entry/Soma_(biology)) (Accessed: 27 April 2018).
- [10] Dietzel, I., Heinemann, U., Hofmeier, G. and Lux, H.D. (1982) 'Stimulus-induced changes in extracellular Na⁺ and Cl⁻ concentration in relation to changes in the size of the extracellular space', *Experimental brain research*, 46(1), pp.73-84.
- [11] Nicholson, C., Ten Bruggencate, G., Stockle, H. and Steinberg, R. (1978) 'Calcium and potassium changes in extracellular microenvironment of cat cerebellar cortex', *Journal of neurophysiology*, 41(4), pp.1026-1039.
- [12] 'Cerebral cortex'(2018) *Wikipedia*. Available at: https://en.wikipedia.org/wiki/Cerebral_cortex (Accessed: 27 April 2018).
- [13] Maier, A., Adams, G.K., Aura, C. and Leopold, D.A. (2010) 'Distinct superficial and deep laminar domains of activity in the visual cortex during rest and stimulation', *Frontiers in systems neuroscience*, 4, p.31.
- [14] Einevoll, G., Linden, H., Tetzlaff, T., Leski, S., Pettersen, K. (2013). *Local Field Potentials: Biophysical Origin and Analysis*, 37-60. Available at: https://www.researchgate.net/publication/281869785\Local_Field_Potentials_Biophysical_Origin_and_Analysis(Accessed: 27 April 2018).
- [15] Solbrå, A., Bergersen, A.W., Brink, J.v.d., Malthe-Sørenssen, A. Einevoll, G.T, Halnes, G.(2018) 'A Kirchhoff–Nernst–Planck framework for modeling large scale extracellular electrodiffusion surrounding morphologically detailed neurons' *bioRxiv* 261107;Available at <https://doi.org/10.1101/261107>
- [16] Halnes, G., Østby, I., Pettersen, K.H., Omholt, S.W. and Einevoll, G.T. (2015) 'An electrodifusive formalism for ion concentration dynamics in excitable cells and the extracellular space surrounding them' *In Advances in cognitive neurodynamics (IV)* (pp. 353-360). Springer, Dordrecht.

- [17] 'Fast Fourier transform'(2018) *Wikipedia*. Available at: https://en.wikipedia.org/wiki/Fast_{Fourier}_transform(Accessed: 27 April 2018)
- [18] 'Tutorial on measurement of power spectra'(2013) *123.physics.ucdavis.edu*. Available at: http://123.physics.ucdavis.edu/week\2\files/tutorial\on\measurement_of_power\spectra.pdf(Accessed: 27 April 2018)
- [19] M. Hjort-Jensen: Computational Physics: Partial Differential Equations, <http://compphysics.github.io/ComputationalPhysics/doc/pub/pde/pdf/pde-print.pdf>
- [20] Oschmann, F., Berry, H., Obermayer, K. and Lenk, K. (2017) 'From in silico astrocyte cell models to neuron-astrocyte network models: A review', *Brain research bulletin*
- [21] Baranauskas, G., Maggiolini, E., Vato, A., Angotzi, G., Bonfanti, A., Zambra, G., Spinelli, A. and Fadiga, L. (2011) 'Origins of 1/f² scaling in the power spectrum of intracortical local field potential', *Journal of Neurophysiology*, 107(3), pp.984-994.
- [22] Jankowski, M.M., Islam, M.N. and O'Mara, S.M. (2017) 'Dynamics of spontaneous local field potentials in the anterior claustrum of freely moving rats', *Brain research*, 1677, pp.101-117.



Norges miljø- og biovitenskapelige universitet
Noregs miljø- og biovitenskapslelege universitet
Norwegian University of Life Sciences

Postboks 5003
NO-1432 Ås
Norway